

# Modeling Coccolithophores in the Global Oceans

Watson W. Gregg  
Global Modeling and Assimilation Office  
NASA/Goddard Space Flight Center  
Greenbelt, MD 20771  
watson.gregg@nasa.gov

Nancy W. Casey  
Science Systems and Applications, Inc.  
Lanham, MD 20706  
nancy.casey@gsfc.nasa.gov

Deep-Sea Research II Special Issue  
Submitted March, 2006  
Revised May, 2006

## **Abstract**

Coccolithophores are important ecological and geochemical components of the global oceans. A global three-dimensional model was used to simulate their distributions in a multi-phytoplankton context. The realism of the simulation was supported by comparisons of model surface nutrients and total chlorophyll with in situ and satellite observations. Nitrate, silica, and dissolved iron surface distributions were positively correlated with in situ data across major oceanographic basins. Global annual departures were +18.9% for nitrate (model high), +5.4% for silica, and +45.0% for iron. Total surface chlorophyll was also positively correlated with satellite and in situ data sets across major basins. Global annual departures were -8.0% with SeaWiFS (model low), +1.1% with Aqua, and -17.1% with in situ data. Global annual primary production estimates were within 1% and 9% of estimates derived from SeaWiFS and Aqua, respectively, using a common primary production algorithm.

Coccolithophore annual mean relative abundances were 2.6% lower than observations, but were positively correlated across basins. Two of the other three phytoplankton groups, diatoms and cyanobacteria, were also positively correlated with observations.

Distributions of coccolithophores were dependent upon interactions and competition with the other phytoplankton groups. In this model coccolithophores had a competitive advantage over diatoms and chlorophytes by virtue of a greater ability to utilize nutrients and light at low values. However, their higher sinking rates placed them at a disadvantage when nutrients and light were

plentiful. In very low nutrient conditions, such as the mid-ocean gyres, coccolithophores were unable to compete with the efficient nutrient utilization capability and low sinking rate of cyanobacteria.

Comparisons of simulated coccolithophore distributions with satellite-derived estimates of calcite concentration and coccolithophore blooms showed some agreement, but also areas of departure. Vast blooms observed in the North Atlantic were well-represented by the model. However, model coccolithophores were nearly absent in the North Pacific, while calcite estimates suggested widespread abundance in summer. In situ observations supported the satellite calcite, suggesting a deficiency in the model. New satellite estimates of phytoplankton groups indicated good agreement of diatoms in one case, and poor agreement in general in another. Comparisons of phytoplankton group primary production with other models showed wide disparity. The divergence among models and satellite estimates is common for such an emerging field of research. The quantitative comparisons with in situ observations were encouraging, but disparities with model and satellite estimates suggested that further research is needed.

## **Introduction**

Coccolithophores are a widespread phytoplankton taxonomic assemblage in the global oceans. They are occasionally abundant in some seasons and regions, and are a primary source of oceanic calcite. As a consequence of their abundance they are important for ocean ecosystems. As a consequence of their production of calcite they are important for ocean geochemistry. In either case understanding their distributions is necessary to expand our knowledge of ocean ecology and biogeochemistry.

There is much recent interest in understanding coccolithophore distributions in the global ocean, from both modeling and satellite perspectives. Moore et al. (2002a; 2004) implicitly assessed coccolithophore distributions as a varying proportion of their small phytoplankton assemblage, one of three prognostic phytoplankton groups. Jin et al. (2006) also implicitly described coccolithophore distributions in a model using a single prognostic phytoplankton component, and then partitioning the total biomass into 5 assemblages, one of which represented coccolithophores.

Tyrrell and Taylor (1996) introduced a prognostic simulation of coccolithophores in a one-dimensional, two-layer model of the Northeast Atlantic. In this four-phytoplankton component representation, coccolithophores differed from other phytoplankton only in half-saturation constants for phosphate (lower) and light (higher). They differed from diatoms in that they did not sink. Gregg et al. (2003) and Le Quéré et al. (2005) provided three-dimensional representations of coccolithophores in the global oceans along with three other phytoplankton assemblages. These explicit, prognostic descriptions of coccolithophores were independent of other phytoplankton characterizations and processes, and included specific characterizations of maximum growth rate, nutrient uptake, light adaptation, and in the case of Gregg et al. (2003), different sinking rates.

Regarding satellite investigations, Balch et al. (2005) used ocean color data to remotely quantify oceanic suspended calcium carbonate, derived primarily from coccolithophores. This represented a breakthrough for quantitative detection from space, building upon pioneering efforts to identify presence (Brown and Yoder, 1994), and probability (Iglesias-Rodriguez et al., 2002) of coccolithophores blooms.

In this effort we seek to 1) simulate distributions of coccolithophores in the global oceans with an explicit, prognostic description of coccolithophores, 2) evaluate the realism of the simulated distributions, and 3) determine causes for the distributions. The simulation is accomplished using an established three-dimensional model of the global oceans containing prognostic representations of three additional phytoplankton groups (diatoms, chlorophytes, cyanobacteria) to evaluate coccolithophore distributions in the context of multiple biological interactions. Evaluation is achieved through comparison with observations of phytoplankton relative abundances, and especially coccolithophore distributions. Discerning causes for the distributions involves model diagnosis both where and when the model is reasonably successful in its representation, and where it is not.

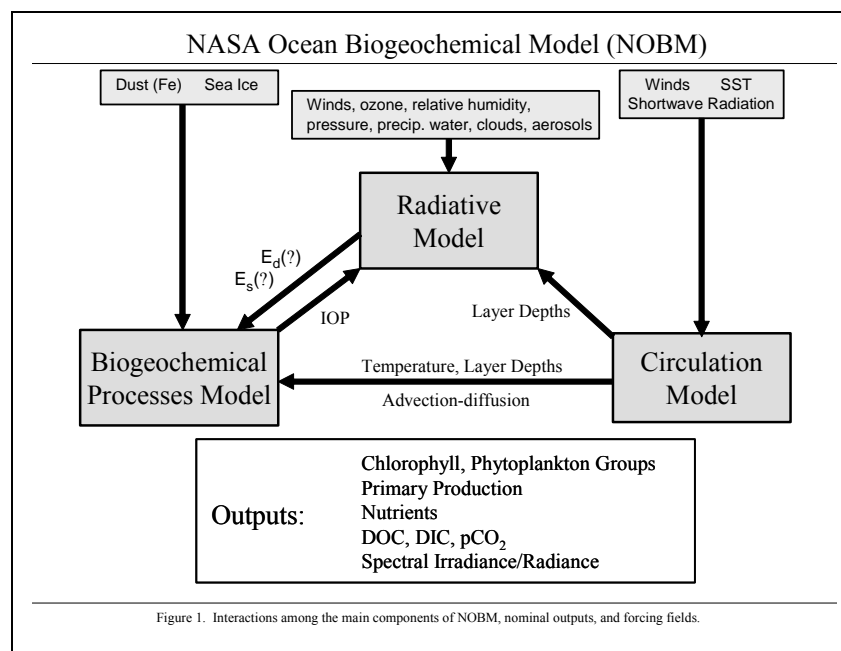
The model described and used here utilizes a taxonomic definition of phytoplankton groups, based primarily on laboratory investigations. However, analysis of results uses a hybrid functional/taxonomic appraisal. Specifically, cyanobacteria represent both diazotrophic genera such as *Trichodesmium* spp. and non-diazotrophic genera such as *Synechococcus* spp. and *Prochlorococcus* spp. The chlorophytes taxonomic group is used to represent a wide range of small eukaryotic phytoplankton, including diverse assemblages of so-called flagellates and

nanoplankton, but more specifically including pelagophytes, prasinophytes, non-coccolithophore prymnesiophytes, cryptomonads, and many others. The diatoms and coccolithophore classifications are strictly taxonomic. Coccolithophore characterizations in the model are primarily for *Emiliana huxleyi*.

This effort is an extension of previous work (Gregg et al., 2003), to include organic and inorganic carbon cycling, and to re-assess results based on the availability of new data on phytoplankton group distributions, both in situ and satellite. In addition, we provide here a more detailed analysis of the model results emphasizing coccolithophores, that we hope can help guide improvements in the global modeling of this important biological constituent as well as other phytoplankton assemblages.

## Methods

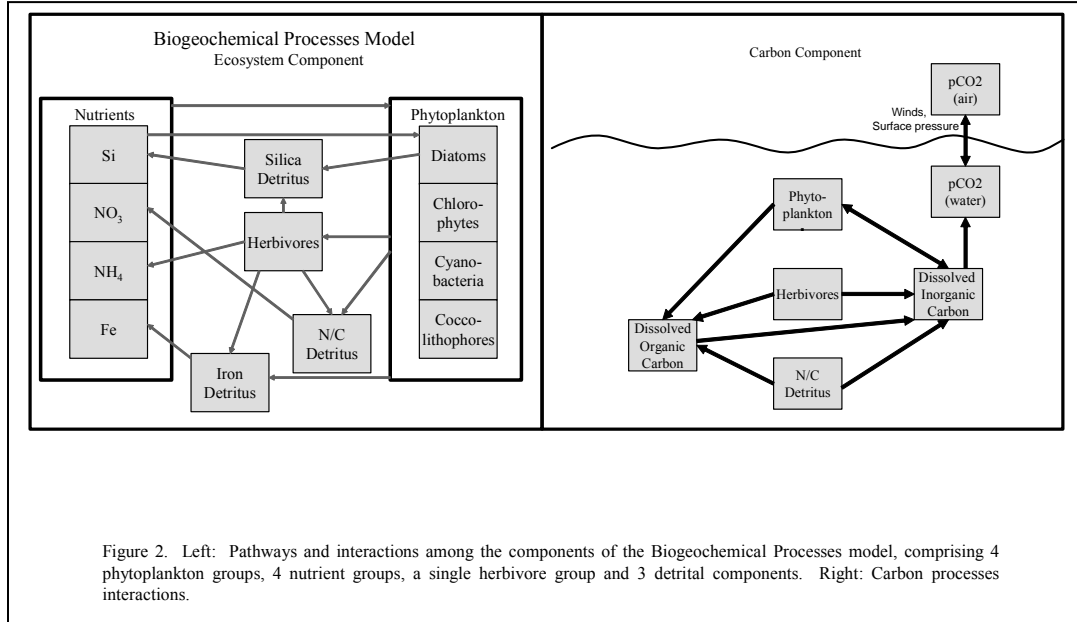
### *Global Three-Dimensional Circulation Model*



The model used in this effort is called the NASA Ocean Biogeochemical Model (NOBM; Figure 1). It is a three-dimensional representation of coupled circulation/biogeochemical/radiative processes in the global oceans. It spans the domain from  $-84^\circ$  to  $72^\circ$  latitude in increments of  $1.25^\circ$  longitude by  $2/3^\circ$

latitude, including only open ocean areas, where bottom depth  $> 200\text{m}$ . A previous version was described in Gregg et al. (2003). The version used here differs primarily in the addition of dissolved inorganic and organic carbon cycling. The biogeochemical processes model contains 4 phytoplankton groups, 4 nutrient groups, a single herbivore group, and 3 detrital pools (Figure 2). The phytoplankton groups differ in maximum growth rates, sinking rates, nutrient requirements, and optical properties. The 4 nutrients are nitrate, regenerated ammonium, silica

to regulate diatom growth, and iron. Three detrital pools provide for storage of organic material,



sinking, and eventual remineralization back to usable nutrients. Carbon cycling involves dissolved organic carbon (DOC) and dissolved inorganic carbon (DIC). DOC has sources from phytoplankton, herbivores, and carbon detritus, and a sink to DIC. DIC has sources from phytoplankton, herbivores, carbon detritus, and DOC, and communicates with the atmosphere, which can be either a source or sink. The ecosystem sink for DIC is phytoplankton, through photosynthesis. A complete description of the parameters in the biogeochemical processes and carbon models, as well as brief descriptions of the general circulation and radiative models, are provided in the Appendix.

## Data Sets

### Forcing Data Sets

Forcing data sets are shown in Figure 1. All except soil dust, ozone, clouds, and atmospheric CO<sub>2</sub> were obtained from National Center for Environmental Prediction Reanalysis products. Ozone was from the Total Ozone Mapping Spectrometer, and soil dust was from Ginoux et al. (2001). Monthly climatologies were used in all cases. Cloud data (cover and liquid water path) were obtained from the International Satellite Cloud Climatology Project. Atmospheric CO<sub>2</sub> was taken from the Ocean Carbon-Cycle Model Intercomparison Project (<http://www.ipsl.jussieu.fr/OCMIP/>; derived from Enting et al., 1994), using the value for the year 2000 as the climatological mean.

### Comparison Data Sets

Global chlorophyll data from the Sea-viewing Wide Field-of-view Sensor (SeaWiFS) and the Moderate Resolution Imaging Spectroradiometer (MODIS)-Aqua were obtained from the NASA Ocean Color Web site at monthly 9-km resolution. The data set version numbers were SeaWiFS V5.1 and Aqua V1.1. The data were re-mapped to the model grid and averaged to monthly climatologies before comparison.

In situ nitrate, silica, and chlorophyll fields were obtained from the National Oceanographic Data Center (NODC; Conkright et al., 2002). Dissolved iron data were taken from Gregg et al. (2003). DIC data were taken from Key et al., (2004). Annual mean data were used for comparison between model results and observations, where mixed layer depth-averages were computed using model annual mean mixed layer depth.

Comparisons utilized the relative percent difference globally and over basins (Figure 3)

$$RPD = \frac{M-D}{D} \times 100 \quad (1)$$

where RPD is the relative percent difference, M is the model value, and D is the data or observation value.

While annual mean data are the simplest and most efficient means to describe comparisons, it should be noted that annual mean nitrate and silica from NODC are used as initial conditions for the model. Comparison after 20 years of simulation (nitrate and silica were re-initialized to

NODC after the first 15 years of the 35-year spinup, see Appendix) is reasonable because the model reached steady state after this integration. However, statistics from seasonal comparisons are also

Table 1. Global mean difference between NOBM and NODC observations (model-data) for nitrate and silica by season, and correlation coefficients (r) across basins. An asterisk indicate a statistically significant correlation (P<0.05).

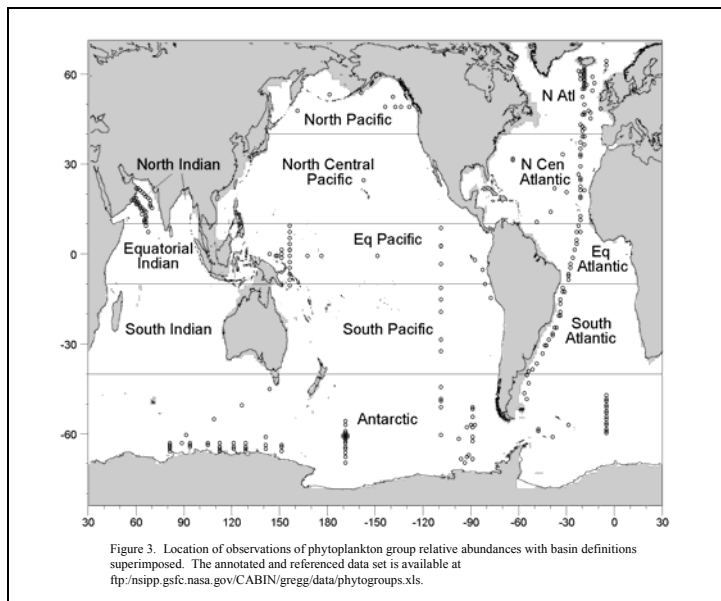
	Nitrate		Silica	
	Difference	r	Difference	r
Winter (Jan-Mar)	21.3%	0.969*	13.3%	0.954*
Spring (Apr-Jun)	21.8%	0.950*	8.8%	0.956*
Summer (Jul-Sep)	18.2%	0.900*	4.9%	0.941*
Autumn (Oct-Dec)	19.1%	0.940*	4.1%	0.958*

provided for additional validation (Table 1).

### Phytoplankton Group Data

We have expanded upon the data set used by Gregg et al. (2003) to include more recent observations. We now have 469 surface layer observations of phytoplankton group abundances (Figure 3), an increase of more than 100. The annotated, fully referenced data are available as an

Excel© spreadsheet at the NASA Global Modeling and Assimilation Office web site <http://polar.gsfc.nasa.gov/research/oceanbiology/index.php>. The sources for the data spreadsheet are, in alphabetical order: Agusti et al., 2001; Andersen et al., 1996; Barlow et al., 1993; 1999; Bathmann et al., 1997; Blanchot et al., 2001; Brown and Landry, 2001; Campbell et al., 1997; Carreto et al., 2003; Claustre and Marty, 1995; DiTullio et al., 2005; DuRand et al., 2001; Everitt et al., 1990; Gall et al., 2001; Garrison et al., 1993; Gibb et al., 2001; Goericke, 2002; Hardy et al., 1996; Harris et al., 1997; Higgins and Mackey, 2000; Holligan et al., 1993; Hutchins et al., 2002; Ishizaka et al., 1997; Lam et al., 2001; Landry et al., 2001; 2002; Letelier et al., 1993; Malin et al., 1993; Maranon et al., 2000; Miller et al., 1991; Obayashi et al., 2001; Peeken, 1997; Steinberg et al., 2001; Tarran et al., 1999; Thibault et al., 1999; van Leeuwe et al., 1997; Veldhuis and Kraay, 2004; Wright et al., 1996; Wright and van Enden, 2000. As in Gregg et al. (2003), data are converted when necessary into percent abundance of the entire population to compare with the model.



In our analysis of the phytoplankton group data, we match up model mixed layer relative abundances with the location and month of the in situ observations. We assemble all of these co-located, coincident match-ups over ocean basins, and over all the months for a year. We then average these match-ups over the basin annually. This provides us an opportunity to observe the large scale spatial performance of the model while keeping a close model-data relationship. We perform correlation analysis using these annual means across the basins to evaluate correspondence of distributions on basin scales. The difference is expressed as model minus observations, unlike Eq. 1, since the values represent the relative abundance in percent.

### **Primary Production**

Primary production is computed in the model as a function of growth rate multiplied by the carbon:chlorophyll ratio:

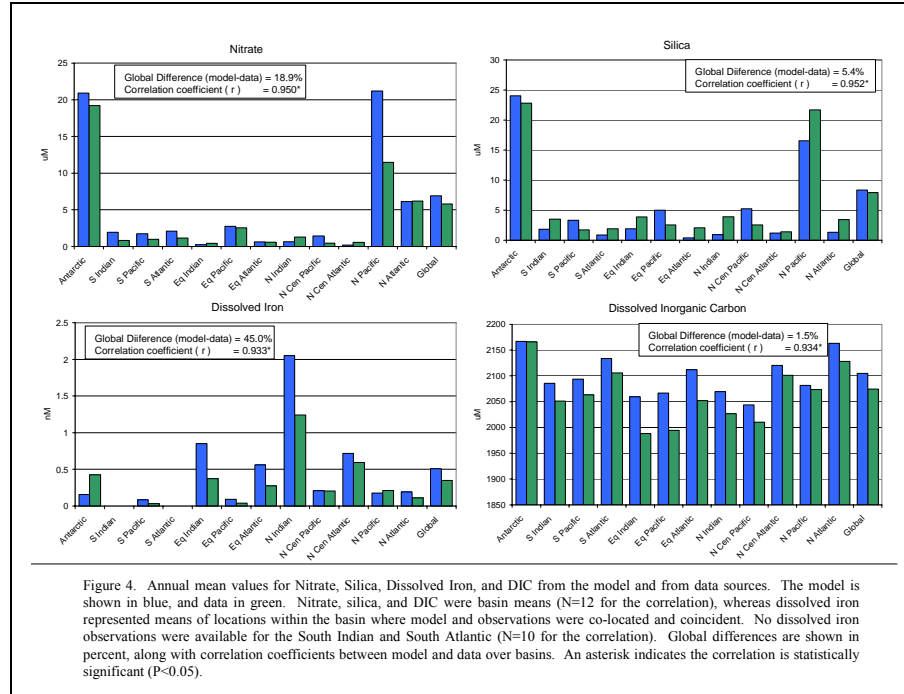
$$PP = \int \sum \mu_i C_i \Phi dz \quad (2)$$

where  $\mu_i$  is the realized new growth rate of phytoplankton component  $i$ ,  $C_i$  is the chlorophyll concentration of component  $i$ ,  $\Phi$  is the carbon:chlorophyll ratio, and the product is integrated over depth. Model-computed primary production is compared with primary production derived directly from satellite chlorophyll data using the Vertically Generalized Production Model (VGPM; Behrenfeld and Falkowski, 1997). The VGPM requires chlorophyll, sea surface temperature (SST), and photosynthetically available radiation (PAR) as inputs. Chlorophyll is taken from SeaWiFS and Aqua, SST is the same source as used for model forcing, and PAR is derived from the atmospheric component of the radiative model, with wavelength region 350-700 nm selected and converted to quanta. Model primary production can be partitioned into contributions from the phytoplankton components ( $PP_i$ ), simply by removing the summation in Eq. 2. VGPM is applied to SeaWiFS, Aqua, and NODC over the model domain.

## Results

### *Comparison of NOBM Nutrients, Inorganic Carbon, and Total Chlorophyll with Data Sets*

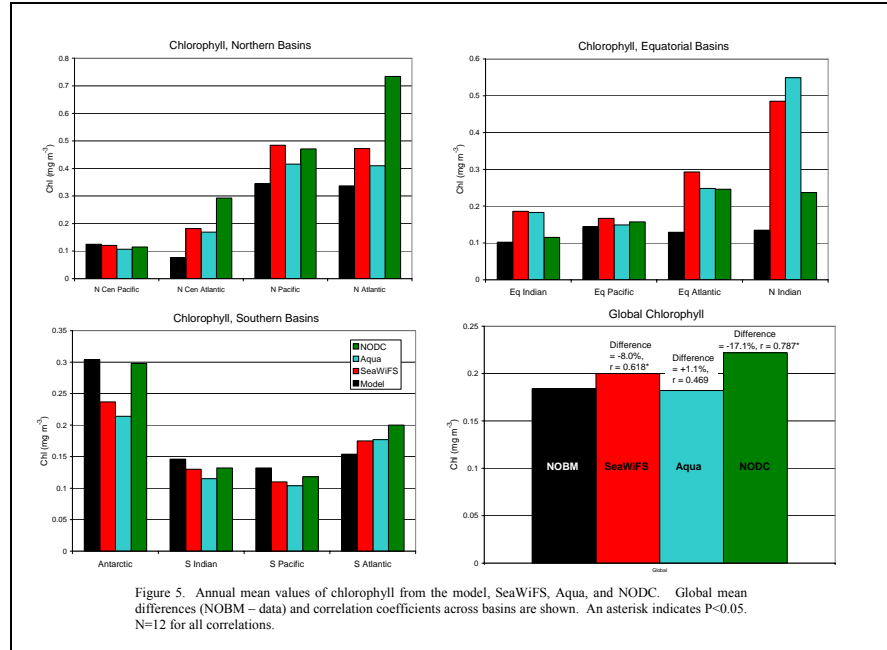
Comparison of basin annual mean nutrients from NOBM with climatological observations indicated overall agreement. Correlation over the basins was statistically significant ( $P < 0.05$ ) for



all nutrients, as well as DIC (Figure 4). Noteworthy departures of the model included excessive nitrate in the North Pacific, a tendency for under-representation of silica in the Atlantic and Indian basins, overestimates of silica except for the North



Pacific, over-representation of dissolved iron in basins near the Saharan desert source region,



underestimation of iron in the Antarctic, and overestimation of DIC in the tropics.

Similar comparisons of model total chlorophyll with SeaWiFS and NODC chlorophyll annual climatologies again indicated positive correlation over basin, with low global mean differences (Figure 5).

Aqua chlorophyll also showed low global mean difference but the basins were not significantly correlated with in situ data. Globally, the NODC chlorophyll exhibited the highest global annual mean, followed by SeaWiFS. NOBM and Aqua had very similar global annual means (Figure 5).

### ***Comparison of Phytoplankton Groups with In Situ Data***

NOBM basin-scale relative abundance distributions of diatoms, cyanobacteria, and coccolithophores were positively correlated with in situ data (Figure 6). Global mean differences of all groups were within 20% of observations. Coccolithophores global mean relative abundance, the emphasis of this effort, was slightly low by 2.6%. NOBM underestimated coccolithophore relative abundances in the North Pacific and Antarctic, in both cases indicating nearly negligible values while substantial relative abundances were reported in the observations. These were incidentally two of the lowest three concentrations of dissolved iron in the model. Modest overestimates by the model in the North Atlantic and the Equatorial Pacific occurred. Both model and data exhibited basin maxima in the North Atlantic, but the minima diverged. The model minima were found in the North Pacific and Antarctic, while the observation minimum occurred in the North Indian. A substantial underestimate in the model also occurred

in the South Atlantic but otherwise distributions were in reasonable agreement, as suggested by

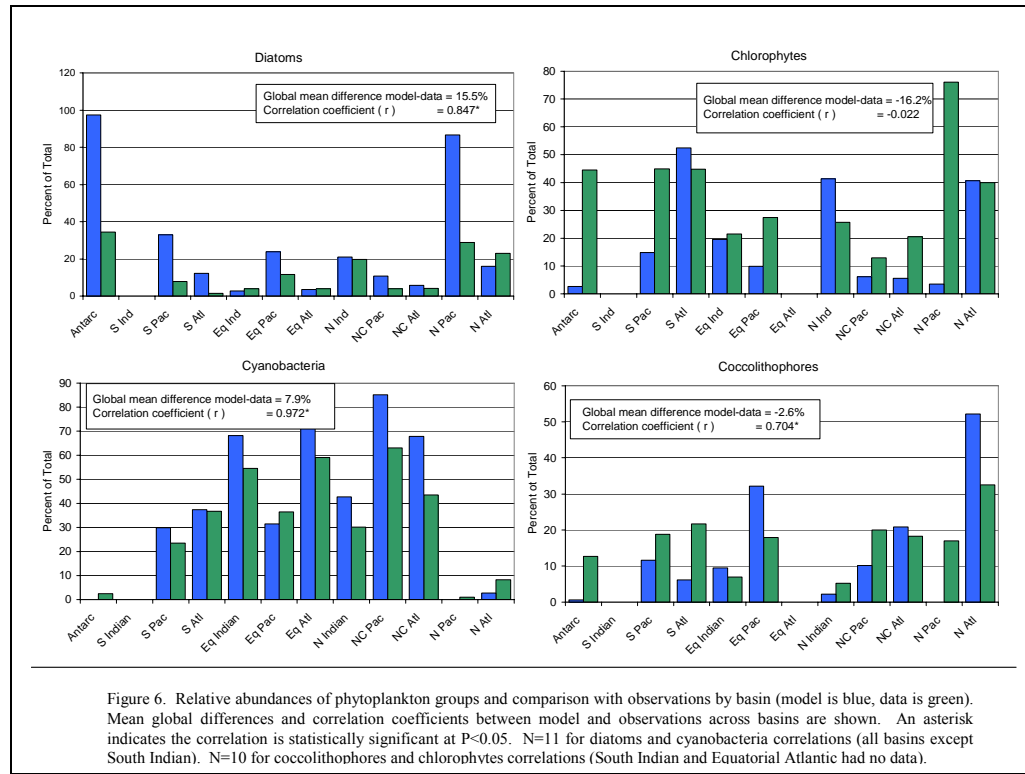


Figure 6. Relative abundances of phytoplankton groups and comparison with observations by basin (model is blue, data is green). Mean global differences and correlation coefficients between model and observations across basins are shown. An asterisk indicates the correlation is statistically significant at  $P < 0.05$ .  $N=11$  for diatoms and cyanobacteria correlations (all basins except South Indian).  $N=10$  for coccolithophores and chlorophytes correlations (South Indian and Equatorial Atlantic had no data).

Antarctic, South Pacific, and South Atlantic, where NOBM overestimated their relative abundance. These were coincidentally the same basins where simulated coccolithophores abundance was low. Except for these basins, agreement between the model and observations was close.

Of all the phytoplankton groups in NOBM, cyanobacteria exhibited the highest correspondence with observations (Figure 6). Very high correlation coefficient over basins (0.972) was coupled with low global mean annual departure (7.9%) and remarkably close agreement basin-by-basin.

Chlorophyte relative abundance distributions represented the maximum departure from observations, at -17.2%, and additionally exhibited no correlation with observations. Particularly striking were underestimates by the model in the North Pacific and Antarctic, which incidentally contained two of the lowest three concentrations of dissolved iron in the model. This was the only group that did not exhibit significant correlation between model and observations.

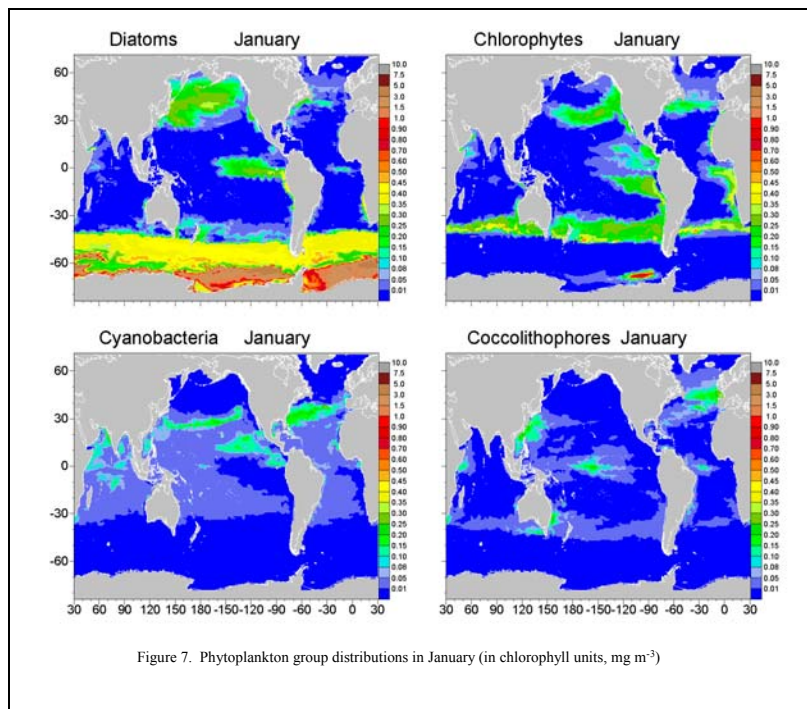
### Phytoplankton Distributions

#### -- Surface

the positive correlation.

Diatoms exhibited a high level of correspondence between the model and observations (Figure 6). The major basins of departure were the North Pacific,

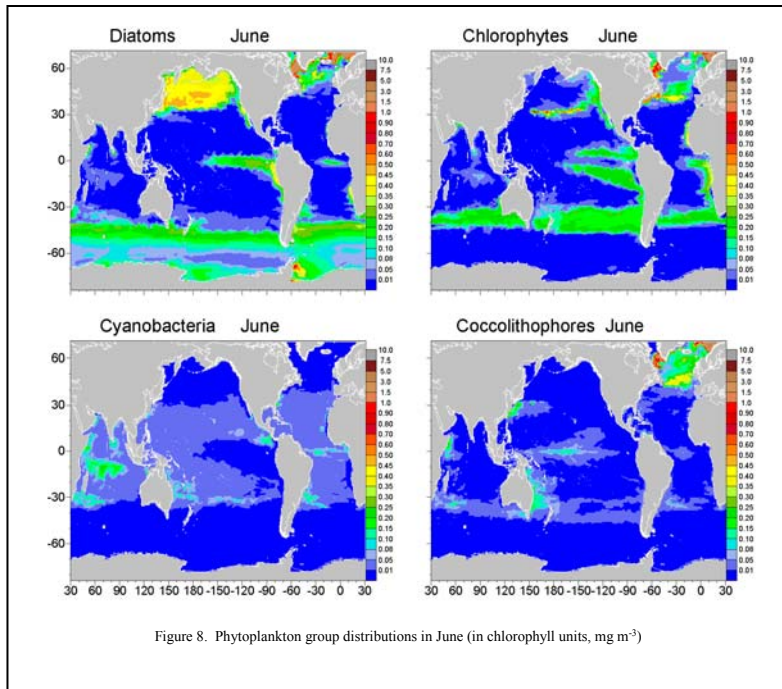
Surface layer distributions in January showed diatom presence in the high latitudes, and in equatorial and coastal upwelling regions (Figure 7). They were absent in and near the central ocean basins, especially the mid-ocean gyres. Cyanobacteria exhibited nearly opposite behavior: presence in the central ocean basins and absence in the high latitudes and upwelling regions. They were abundant in the tropical and northern Indian Ocean. Coccolithophores were abundant in the northern portion of the North Central Atlantic and southern portion of the North Atlantic. They were also found in the central-to-western portions of the tropical basins. Moderately high values were found in the western North Central Pacific near China, and in the Tasman Sea and west of Tasmania. Modest abundances were located in the transition zone between the abundant diatoms in the Antarctic and the abundant cyanobacteria in the southern central gyres. Chlorophytes filled a transitional role, especially around the diatoms in the equatorial upwelling zones and the high latitude/central gyre transition zones in both hemispheres. They were also prevalent in the eastern Equatorial Atlantic.



In June overall surface distributions were similar to January, except abundances were hemispherically reversed (Figure 8). The coccolithophores bloom intensified in the Tasman Sea, and a new bloom occurred in the southwestern South Indian Ocean south of Madagascar, which was shared with cyanobacteria.

Coccolithophores also intensified in the western Indian basins, offshore of Somalia. Coccolithophores, diatoms, and chlorophytes were abundant in the North Atlantic, but only diatoms and chlorophytes were prevalent in the North Pacific. Chlorophytes occupied the eastern portion of the North Pacific while diatoms were prevalent in the western portion.

Phytoplankton group dominance was defined as the group with the largest relative abundance in any model location (grid point). Plots of dominance provided a different perspective on the inter-group competition for nutrient and light. Seasonal distributions showed areas where large changes occurred, but also several that were constant (Figure 9). Diatoms always dominated the axis of the Equatorial Pacific upwelling zone, the Antarctic, and the Namibian coastal upwelling region. Cyanobacteria always dominated the central oceans, especially the gyres. Chlorophytes always dominated the transition zones between high latitudes and central oceans, and equatorial upwelling and central oceans. Coccolithophores always dominated the western end of the Pacific upwelling, the western portion of the South Pacific near Australia, and at least some part of the North Atlantic.

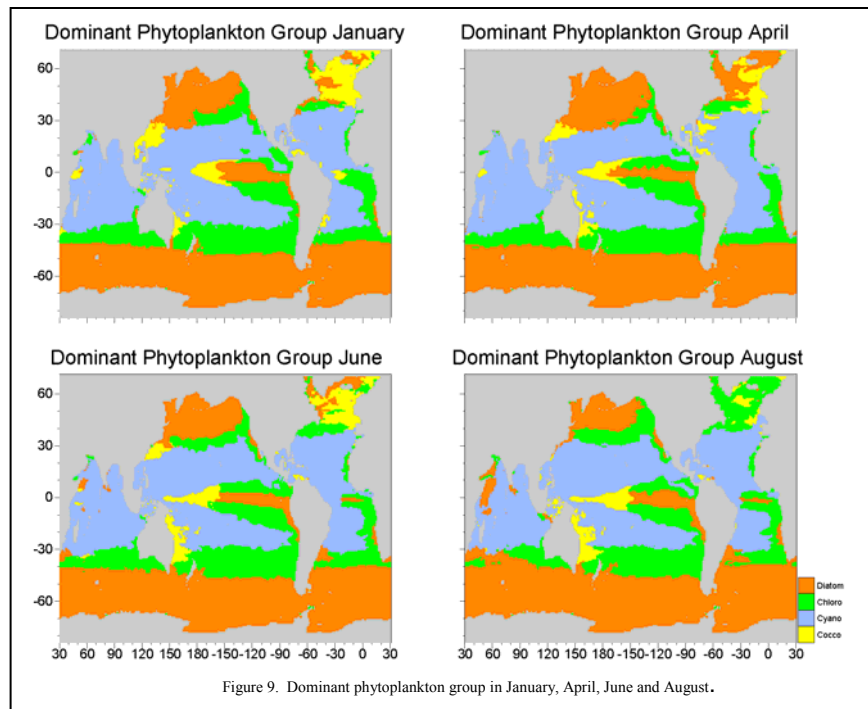


The largest seasonal changes in dominant group occurred in the North Pacific and Atlantic, the western portions of the North and Equatorial Indian, and the Equatorial Atlantic (Figure 9). The North Pacific was always dominated by diatoms in the west and chlorophytes in the east, but seasonal patterns, such as the spring bloom, were associated with encroachment by diatoms

over chlorophytes over much of the eastern part. Diatoms receded after the bloom in August.

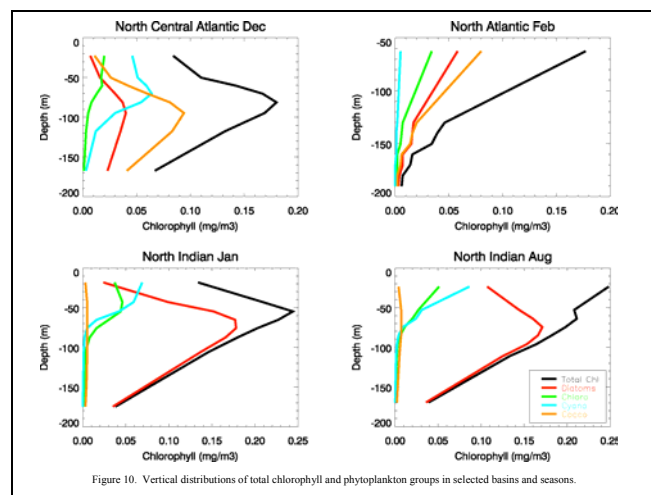
The western North and Equatorial Indian basins were dominated by cyanobacteria in January, with a portion of the northern Arabian Sea occupied by chlorophytes and the near-coastal central portion of the Equatorial Indian dominated by coccolithophores (Figure 9). Minor areas of dominance by diatoms at the mouth of the Red Sea disappeared by April (inter-monsoon). In June areas of diatom dominance expanded and by August (southwest monsoon) had covered nearly the entire western portion of the basins and also the tip of India near Sri Lanka. Small areas of coccolithophore dominance disappeared in August.

The most dynamic basin for seasonal phytoplankton group dominance was the North Atlantic (Figure 9). Here coccolithophores dominated the basin at large during January, with relatively minor patches of dominance by diatoms and chlorophytes interspersed. April, the beginning of the spring bloom, saw major expansion of areas of diatom dominance accompanied by retreat of coccolithophores. June exhibited a reversal as coccolithophores regained dominance over diatoms, with minor expansion of chlorophyte-dominated areas. By August, chlorophytes asserted dominance of most of the basin while diatom-dominated areas were few and small.



#### -- Vertical Distributions

Vertical distributions of the phytoplankton groups exhibited two major patterns: all populations decreasing with depth, and some forming deep chlorophyll maxima (Figure 10). The North



Atlantic in February was an example of the former; in this case all 4 phytoplankton groups decreasing with depth at nearly the same rate. The North Central Atlantic in December, conversely, showed a very strong deep chlorophyll maximum produced mostly by deep coccolithophores but also to a more minor extent cyanobacteria and diatoms.

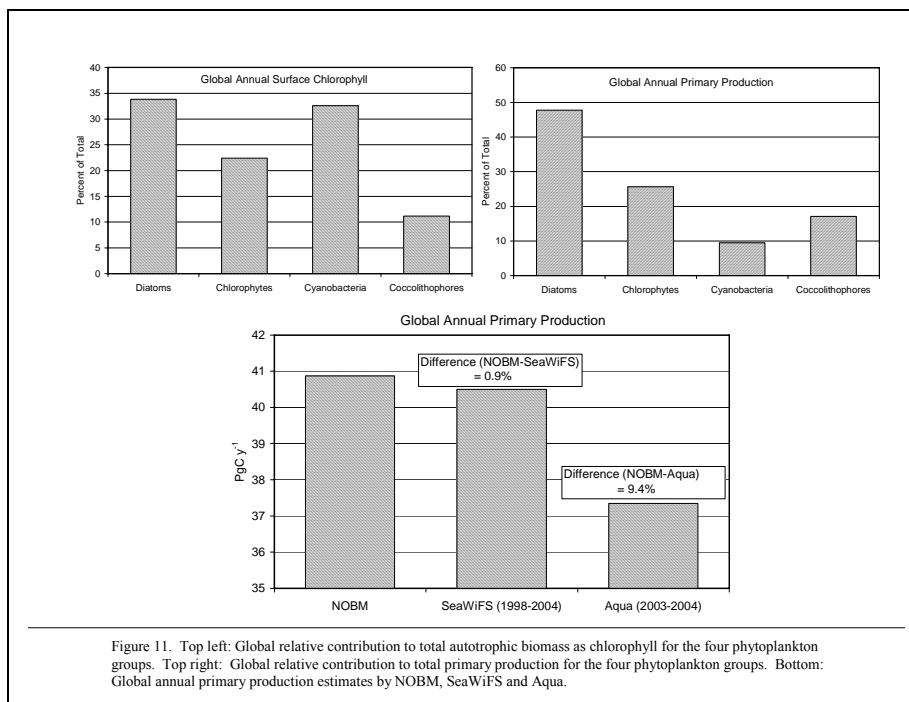
The North Indian Ocean showed how the

deep chlorophyll structure could change by season (Figure 10). At the beginning of the inter-monsoon season in January, a prominent deep chlorophyll maximum was apparent, formed primarily by deep-living diatoms. The dominant surface group was cyanobacteria. In the southwest monsoon period in August, diatoms still predominated at depth, but also at the surface. A declining profile of total chlorophyll with depth was apparent.

### ***Global Surface Relative Abundances and Primary Production Partitioning***

Global surface relative abundances indicated that diatoms contributed nearly 34% of the total phytoplankton biomass as chlorophyll, followed by cyanobacteria at 33%, and finally chlorophytes at 22% (Figure 11). Coccolithophores contributed the least to the total biomass at 11%.

Although diatoms provided only about a third of the global biomass, they contributed nearly half (47.8%) of the global depth-integrated primary production (Figure 11). Cyanobacteria contributed only 9.5% of the primary production, the lowest, in contrast to their one-third contribution to global biomass (co-equal with diatoms). Chlorophytes were the second largest contributor to primary production, at about 25.6%, and coccolithophores were third at 17.1%.

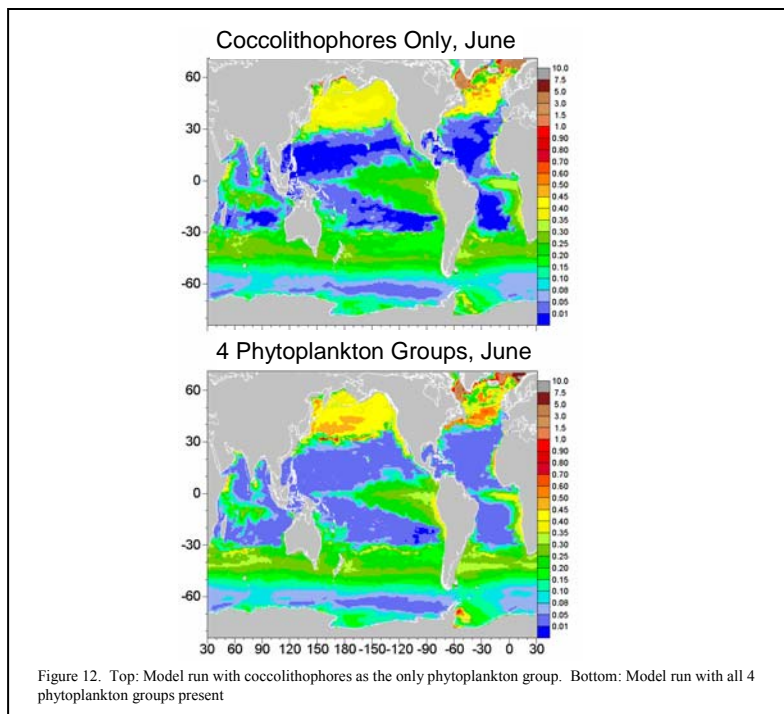


Global annual primary production estimates by NOBM were nearly identical to estimates by VGPM using SeaWiFS chlorophyll over the NOBM domain, 40.9 and 40.5  $\text{PgC y}^{-1}$ , respectively (Figure 11). Primary production estimated by VGPM-Aqua was slightly lower at 37.3  $\text{PgC y}^{-1}$ , but within about 9% of the model and 8% of VGPM-SeaWiFS.



## Discussion

Coccolithophore distributions in the global oceans must be assessed in the context of other phytoplankton. Competition for light and nutrients with other phytoplankton strongly determines where and when coccolithophores flourish or fail. A clear example of this is a test where coccolithophores were the only phytoplankton group present (Figure 12). In this case coccolithophores occupied nearly all the same ocean areas with nearly the same abundances as the 4-component assemblage.



In the configuration of NOBM, if plentiful nutrients and light are provided, diatoms will dominate. This is because of their high maximum growth rate (highest of all groups, see Appendix Table 1). At the other extreme, when nutrients are at exceedingly low concentrations, cyanobacteria will dominate, because of their small size and consequent low sinking rate, as well as their ability to utilize nutrients

efficiently at low amounts (i.e., low half-saturation constants, see Appendix Table 1). These two conditions represent the most clearly defined niches in the model.

In the middle ground, the transition areas between these extremes, a life-or-death competition exists between chlorophytes and coccolithophores, as well as extended ranges of diatoms and cyanobacteria. These niches are less clearly defined than the ones dominated by diatoms and cyanobacteria. To prevail in these regions, coccolithophores need some competitive advantages.

Coccolithophores inhabit a unique niche in the model. They are third of four in maximum growth rate (cyanobacteria are slowest, see Appendix), and they have a high sinking rate. These attributes tend to put them at a competitive disadvantage with respect to diatoms and chlorophytes (growth rate) and cyanobacteria (sinking rate). However, their low nitrate and dissolved iron half-saturation constants enable them to more efficiently utilize nutrients in

reduced concentrations, and their low light saturation parameter for low irradiances helps them use light more effectively. These attributes give them a competitive advantage over the other groups under specific conditions. The key to their success in the global oceans is to find areas where nutrients and light are low enough to inhibit growth by diatoms and chlorophytes, but where there is sufficient vertical mixing to prevent their sinking losses from overtaking them, or where they can find nutrients at depth under low illumination levels.

### ***Coccolithophore Distributions: Comparison with Observations***

Considering the competitive environment of the global ocean ecosystems, some of which appears to be represented in this multi-phytoplankton simulation, it is encouraging that we have achieved some success in modeling the distributions of coccolithophores, as compared to a sparse but wide-ranging in situ data archive. Their abundance in the North Atlantic is confirmed by several investigators (e.g., Okada and McIntyre, 1979; Robertson et al., 1994; Boyd et al., 1997; Balestra et al., 2004). Here, coccolithophores reach their greatest abundance and largest spatial dominance in the global oceans, as determined by observations and the model. Here, their nutrient scavenging abilities are well-utilized, as diatoms use up the available silica at the peak of the spring bloom. This gives rise to a contest between coccolithophores and chlorophytes, which is won initially by coccolithophores by virtue of their high growth capability (third highest) and superior nutrient scavenging, until their higher sinking rates overtake them.

A major deficiency in the model is the near absence of coccolithophores in the North Pacific, especially the eastern portion. This portion, frequently classified as one of the major High Nutrient Low Chlorophyll (HNLC) regions of the oceans (Crawford et al., 2003) because of iron-limitation during certain times of year (Martin and Fitzwater, 1988) has been reported to contain coccolithophores in substantial amounts (Okada and Honjo, 1973; Lam et al., 2001; Crawford et al., 2003), and large amounts of calcite production have been estimated from satellite (Balch et al., 2005). Estimated blooms from ocean color satellites (Brown and Yoder, 1994; Iglesias-Rodriguez et al., 2002), however, have been scarce here. In NOBM, iron limitation inhibits drawdown of nitrate and silica, thus favoring diatoms and chlorophytes. Although coccolithophores are better able to utilize iron at low concentrations, there is too much iron to give them a competitive advantage. Yet NOBM iron is lower than observations here (Figure 4). Sensitivity studies showed that dissolved iron concentrations of 0.05nM were required to confer a competitive advantage upon coccolithophores, in contrast to the 0.17nM mean annual



concentrations found in the model. Ironically, modest iron limitation provides an advantage to diatoms and chlorophytes by inhibiting silica and nitrate consumption.

Another region of disagreement between NOBM and data is the Equatorial Pacific, where the model indicated that coccolithophores dominated the phytoplankton at the distal (western) end of the upwelling region, beyond the area of dominance by diatoms. In the model the dynamics are similar to the North Atlantic: diatoms dominate when the nutrients are plentiful, in the eastern and axial portions of the upwelling, giving way to coccolithophores when the nutrients begin to become depleted. DiTullio et al. (2003) reported negligible abundances here and Ishizaka et al. (1997) found low relative abundances here (<10%). Conversely, Okada and Honjo (1973) and Hagino et al. (2000) found abundant and diverse assemblages of coccolithophores here (relative abundances with respect to total chlorophyll or other groups were not available).

The model was also apparently deficient in its representation of coccolithophores in the Southern Ocean (Figure 6). All of the large abundances in observations south of  $-50^{\circ}$  latitude were reported by Wright and van den Enden (2000) using interpretation of HPLC results, often in water  $<2^{\circ}\text{C}$ . Wright et al. (1996) did not find coccolithophores south of  $-53^{\circ}$ . Winter et al. (1999) found coccolithophores as far south as  $-71^{\circ}$ , but noted that this was a rare event. Other investigators have assumed that coccolithophores are rare in very cold Southern Ocean waters in modeling studies (Moore et al., 2004) and satellite estimates (Kamykowski et al., 2002).

The study of phytoplankton distributions has been accelerated recently by the advent of HPLC technology. However, there remains debate on interpreting results, i.e., using pigment analysis to estimate phytoplankton group partitioning (Wright et al., 1996). This can complicate comparison of model results with in situ observations. Additionally, when comparing to models, one encounters a severe form of spatial mismatches, where the observation consists of a sample from a bottle and the model a mean over a grid point typically 10's of km or more in size. This is a problem ocean color scientists have grappled with for many years when validating chlorophyll and radiance results. Temporal mismatches, resulting from a model driven by climatological forcing and observations with localized time-varying conditions, also present problems. Comparing observations and modeled phytoplankton is also a complicated problem because analysis of relative abundances is not independent of phytoplankton group. Mismatches in one of the groups can, and often does, lead to problems representing other groups. Finally, the availability of data to compare with models is still scarce. We have yet to find

quantitative observations of relative abundances in the South Indian and very few in the South Pacific. For all of these reasons, in situ–model comparisons are not necessarily compelling. However, application of statistical probability analysis to these few comparisons lends confidence in our results because it is very difficult to achieve statistical significance at a probability of 95% when the sample size is low.

### ***Comparisons of Primary Production Partitioning with Other Models***

Global annual primary production estimates from NOBM compare favorably with satellite data sets (Figure 11), 40.9 PgC y<sup>-1</sup>, i.e., within 1% of SeaWiFS and 9% of Aqua. Other global models have reported similar values: Aumont et al. (2003): 42.6 PgC y<sup>-1</sup>; Moore et al. (2002b): 45.3 PgC y<sup>-1</sup>; Moore et al. (2004): 48.2 PgC y<sup>-1</sup>; Jin et al. (2006): 78 PgC y<sup>-1</sup>; Dutkiewicz et al. (2005): 35 PgC y<sup>-1</sup>. Global annual values for all of these models represent primarily open ocean estimates, because of their spatial resolution, and are thus lower than those that might be computed from full global SeaWiFS and Aqua estimates. Note that in addition, the NOBM, SeaWiFS, and Aqua values reported here are for the NOBM grid, the most northern latitude for which is 72°N. The values presented here are not necessarily directly inter-comparable; rather, the intent is merely show reasonable convergence in estimates.

More interesting for the purposes of this effort is to compare partitioning of total primary production among phytoplankton groups. There are several global models that contain a representation of phytoplankton groups, and provide this partitioning information. Each model contains different phytoplankton representations, with the exception of diatoms, which are included in all the models.

Clearly the models diverge with respect to estimates of primary production by diatoms (Table 2). NOBM is the high outlier at 48%. Moore et al. (2004) is the next closest at 32%. Our in situ-model comparisons indicate that NOBM overestimates diatom biomass (Figure 6), which

Table 2. Comparison of global annual primary production partitioned by phytoplankton group in several models. A dash indicates that the model does not use the phytoplankton category. NR indicates that the category was not reported by the investigator.

Primary Production	Diatoms	Large Phyto	Small Phyto	Chloro	Cyano	Diaz	Cocco
NOBM	48%	--	--	26%	10%	--	17%
Aumont et al. (2003)	19%	--	--	--	--	--	--
Jin et al. (2006)	14%	31%	68%	--	--	NR	1%
Moore et al. (2004)	32%	--	NR	--	--	0.5%	1-4%
Moore et al. (2002b)	--	24%	75%	--	--	0.5%	NR

coupled with their high maximum growth and depth-distribution (Figure 10), leads to high primary production. However, if the “other large phytoplankton” and diatom categories of Jin et

al. (2006) are combined (“Large Phyto” category in Table 2), their estimates of large phytoplankton production are closer to NOBM, and to Moore et al. (2004) as well. Jin et al. (2006) found that the majority of global annual primary production was contributed by their small phytoplankton category, which functionally most closely aligns with our chlorophyte group. NOBM chlorophyte production is less than half the small phytoplankton estimates by Jin et al. (2006). Our estimates of chlorophyte biomass are low compared to observations by about 16% (Figure 6), which suggests our chlorophyte primary production fraction is low also. But the discrepancy is too large to be explained by low NOBM chlorophytes. A very large disagreement between Jin et al. (2006) and NOBM occurs for coccolithophores, where NOBM indicates primary production contribution of 17% compared to 1% for Jin et al. (2006) and 1-4% for Moore et al. (2004). Our global estimate of coccolithophore biomass compares favorably with observations (Figure 6).

### ***Comparisons of Phytoplankton Groups with Satellite Estimates***

New estimates of phytoplankton groups using ocean color satellites provide an additional comparison for NOBM. These estimates are very recent, and consequently the results must be viewed with caution. Comparisons with model results are not intended to be conclusive, in contrast to the in situ comparisons, but rather of a preliminary and broad sense.

Unfortunately, the new satellite-based estimates do not yet involve coccolithophores directly, but since the simulated distributions of coccolithophores here depends largely on the distribution of other phytoplankton, it makes for yet another potential marker of NOBM performance. As with models, partitioning of phytoplankton groups by satellites differs from NOBM, from each other, and from other models, which unfortunately limits the usefulness of the comparison. In fact, we have not yet found two classification systems that are even similar, except for diatoms.

The most recent estimates from satellite involve the representation of calcite concentration from MODIS Terra (Balch et al., 2005). In this methodology, calcite is assumed to be derived primarily from coccolithophores, so the distributions may provide an implicit description of coccolithophore abundances. It is not clear how valid any relationship between calcite and coccolithophores is, but is presented here in a qualitative fashion.

When compared to NOBM (Figure 13), there is good agreement in the North Atlantic spring bloom. This is also supported by estimates of coccolithophore blooms using SeaWiFS (Figure 14). The bloom fades by summer in NOBM but persists in calcite estimates.

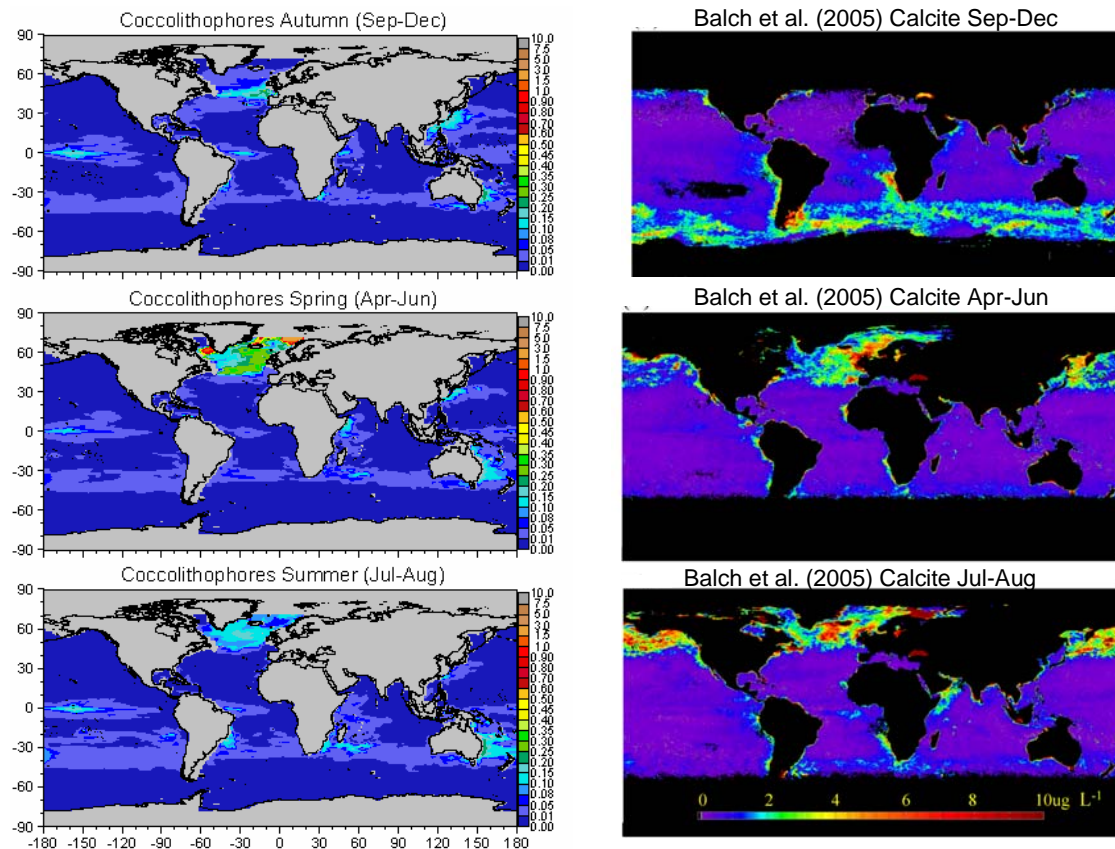


Figure 13. Comparison of coccolithophore distributions from NOBM ( $\text{mg m}^{-3}$ ) and calcite concentrations from MODIS-Terra from Balch et al., (2005), with author's permission.

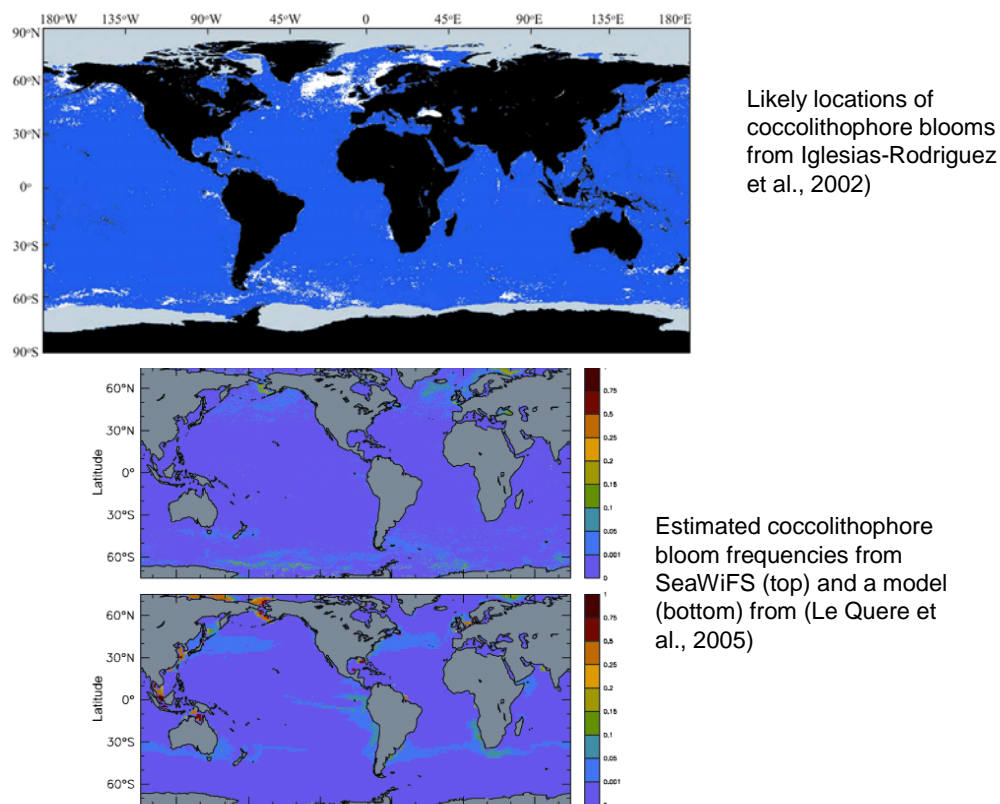


Figure 14. Three estimates of coccolithophore blooms: Top: Likely locations of coccolithophore blooms estimated from environmental variables (top) from Iglesias-Rodriguez et al (2002, with author's permission). Middle: Estimated coccolithophore bloom frequencies from SeaWiFS (from C. Brown, NOAA, with permission, reprinted from Le Quere et al., 2005). Bottom: estimated bloom frequencies from the Dynamic Green Ocean Model (Le Quere et al., 2005, with author's permission).

There is also agreement between NOBM and Balch et al. (2005) in the Southern Ocean transition region, around  $-40^{\circ}$  in the Atlantic and Indian basins. Moderate abundances in the Tasman Sea and southern Australia are apparent in both, more so in NOBM. Modeling estimates from the PlankTOM5 Dynamic Green Ocean Model (Le Quéré et al., 2005) support these distributions. Beyond this, there is rather poor agreement.

Widespread massive concentrations of calcite in the extremes of the Southern Ocean (Figure 13) are nonexistent in the model. Recall that occurrences of coccolithophores in the southern portions of the Antarctic are considered uncommon and even rare by in situ investigators. Brown's estimates of coccolithophore bloom frequency using SeaWiFS (Figure 14) support the Balch et al. (2005) calcite.

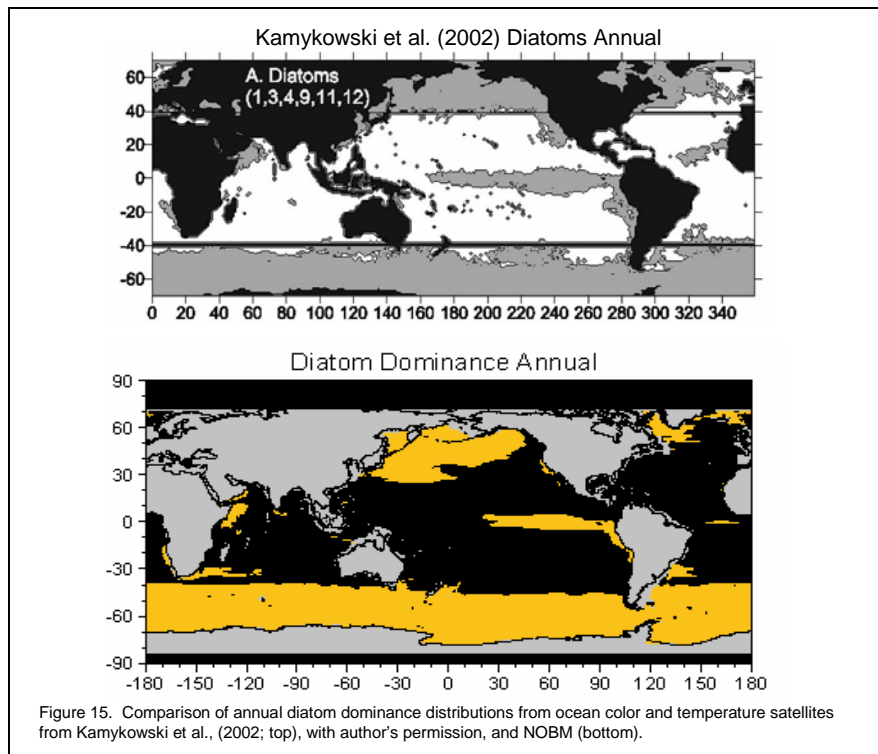
There is no evidence of elevated calcite off the east coast of China or the central Equatorial Pacific, where they flourish in the model. Yang et al. (2001) found large abundances offshore of the China Sea and in the Kuroshio extension northeast of Taiwan. As noted earlier, Hagino et al. (2000) found coccolithophores in abundance in the central-western portions of the Equatorial Pacific, while DiTullio et al. (2003) did not. It is difficult to reconcile these findings.

The largest and most obvious discrepancy between NOBM coccolithophores and Balch et al., (2005) calcite is in the North Pacific (Figure 13) in summer. While the massive nature of the calcite is not supported by coccolithophores bloom frequencies by SeaWiFS and other models (Figure 14), the absence of coccolithophores in NOBM is a clear deficiency. Calcite does not appear in high concentration until summer (well after the spring bloom) and it is distributed around the northern rim of the basin, deriving apparently from the basin margin in spring. This suggests a coastal source for coccolithophores. Perhaps extension of NOBM into shallower ocean regions will help alleviate the model deficiency here. Climatological forcing of the model may also be a factor in play here.

There are two recent estimates of other phytoplankton groups from space. Considering that the simulated distribution of coccolithophores largely depends upon the realism of the simulation of other phytoplankton groups, it is instructive to compare. Again caution should be exercised when evaluating the quality of the comparisons.

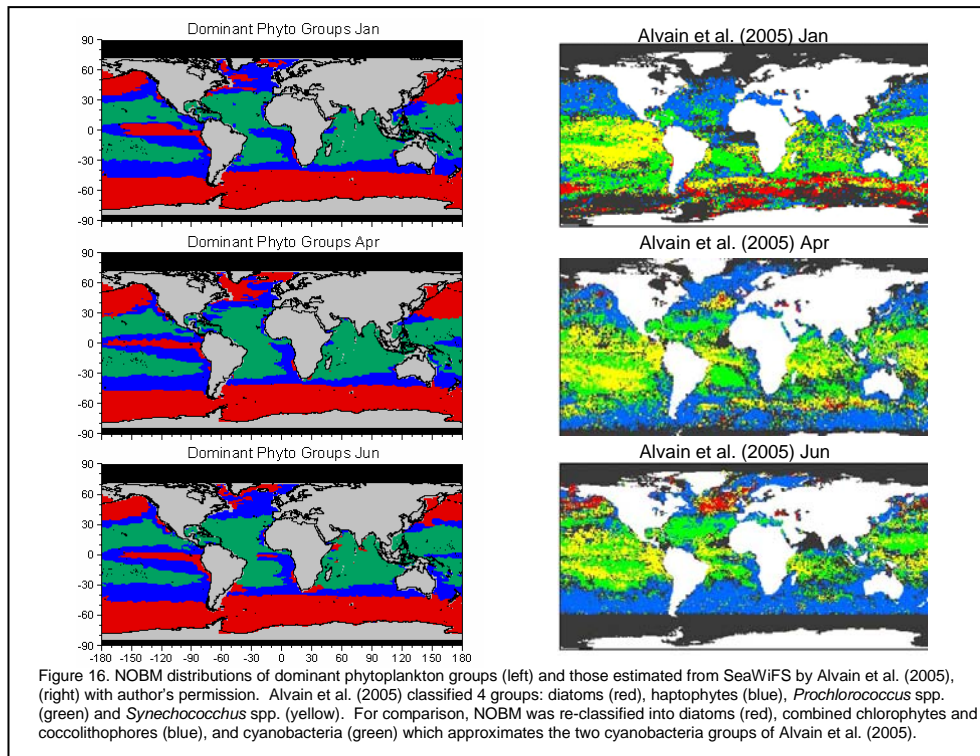
Kamykowski et al., (2002) estimated diatoms, nitrogen fixers, and oligotrophic phytoplankton using a combination of ocean color and temperature remote sensing data. The latter two groups

do not correspond well with NOBM, but the distribution of diatom-dominated areas agrees remarkably well with the model (Figure 15).



This is in contrast to another effort using SeaWiFS to estimate dominance by diatoms, haptophytes, *Prochlorococcus* spp. and *Synechococcus*-like phytoplankton (Alvain et al., 2005). Again the classifications make comparisons cumbersome and only approximate. However, clearly the distribution of diatom dominance by Alvain et

al. (2005) is in contrast to both NOBM and Kamykowski et al. (2002) (Figure 16). Alvain et al. (2005) suggested very limited regions of dominance, and only occurring during the season of local spring bloom. There are major areas of agreement with respect to cyanobacteria, especially in the Indian Ocean. Generally, however, there is little agreement between NOBM and Alvain et al., (2005) for phytoplankton types, even considering the differences in classification. Alvain et al. (2005) show intermingling between *Synechococcus* spp. and diatoms occasionally, whereas in NOBM the diatoms and cyanobacteria never overlap in dominance. Alvain et al. (2005) exhibit a clear hemispheric adjustment by season, but major biogeographic regimes, such as equatorial upwelling and mid-ocean gyres, are not discernible in the dominant phytoplankton groups. NOBM shows clear biogeography, but seasonal hemispheric changes are suppressed in the dominant phytoplankton.



## Summary

Modeling coccolithophores distributions prognostically in a global three-dimensional model with multiple phytoplankton groups is a challenge. This is primarily because the distribution of coccolithophores depends on the simulation of other groups. In ecological terms, competition for nutrients and light is the main determinant of coccolithophores distributions. In analysis terms, this means that their abundances are not independent. Failure or success in replicating coccolithophore distributions depends upon whether all groups are simulated correctly.

Our approach here was to rely heavily on in situ data sets, recognizing their sparseness, the debates about interpretation, and conflicting results. Achieving statistically significant correlations for coccolithophores across broad regions provides some level of confidence in the results. There are clear areas of agreement in diverse satellite estimates as well, particularly the North Atlantic, where most signs point to vary large abundance, and even dominance in some seasons, of coccolithophores. Results elsewhere must be considered mixed, but the present effort has strong grounding in statistical analysis.

The challenges in modeling coccolithophores, however daunting, are important to undertake because of their dual roles in ocean ecology and geochemistry. At a minimum this effort stands

as a step in the direction of prognostic modeling, and the statistical analysis of observations stands as a step toward confirmation. Comparison with other modeling and satellite approaches provides a picture of much disagreement, but also some convergence. It is hoped that this effort plays a role in increasing our understanding the global distributions of coccolithophores, some of the factors affecting them, and suggests directions for improvement.

### **Acknowledgements**

We thank the National Oceanographic Data Center, the NASA Ocean Biology Processing Group, and Global Data Analysis Project for data sets used in this paper. We also thank William Balch, Christopher Brown, Daniel Kamykowski, Débora Iglesias-Rodriguez, Corinne LeQuéré, and Cyril Moulin for permission to use figures for comparison. This work was supported by NASA Grant 621-85-08-20.



## References

- Agawin, N.S.R., C.M. Duarte, and S. Agusti, 1998. Growth and abundance of *Synechococcus* sp. in a Mediterranean Bay: Seasonality and relationship with temperature. *Marine Ecology Progress Series* 170, 45-53.
- Agawin, N.S.R., C.M. Duarte, and S. Agusti, 2000. Nutrient and temperature control of the contribution of picoplankton to phytoplankton biomass and production. *Limnology and Oceanography* 45, 591-600.
- Agusti, S., C.M. Duarte, D. Vaque, M. Hein, J.M. Gasol, and M. Vidal, 2001. Food-web structure and elemental (C, N and P) fluxes in the eastern tropical North Atlantic. *Deep-Sea Research II*, 48, 2295-2321.
- Ahn, Y.-H., A. Bricaud, and A. Morel, 1992. Light backscattering efficiency and related properties of some phytoplankters. *Deep-Sea Res.* 39: 1835-1855.
- Alvain, S., C. Moulin, Y. Dandonneau, and F.M. Breon, 2005. Remote sensing of phytoplankton groups in case 1 waters from global SeaWiFS imagery. *Deep-Sea Research I* 52: 1989-2004.
- Andersen, R.A., R.R. Bidigare, M.D. Keller, and M. Latasa, 1996. A comparison of HPLC pigment signatures and electron microscopic observations for oligotrophic waters of the North Atlantic and Pacific Oceans. *Deep-Sea Research II*, 43, 517-537.
- Anning, T., H.L. MacIntyre, S.M. Pratt, P.J. Sammes, S. Gibb, and R.J. Geider, 2000. Photoacclimation in the marine diatom *Skeletonema costatum*. *Limnology and Oceanography*, 45, 1807-1817.
- Archer, D.E. and K. Johnson, 2000. A model of the iron cycle in the ocean. *Global Biogeochemical Cycles*, 14, 269-279.
- Aumont, O., S. Belviso, and P. Monfray, 2002. Dimethylsulfoniopropionate (DMSP) and dimethylsulfide (DMS) sea surface distributions simulated from a global three-dimensional ocean carbon cycle model. *Journal of Geophysical Research* 107: doi: 10.1029/1999JC000111.
- Aumont, O., E. Maier-Reimer, S. Blain, and P. Monfray, 2003. An ecosystem model of the global ocean including Fe, Si, P colimitations. *Global Biogeochemical Cycles* 17 doi:10.1029/2001gb001745.
- Balch, W.M., H.R. Gordon, B.C. Bowler, D.T. Drapeau, and E.S. Booth, 2005. Calcium carbonate measurements in the surface global ocean based on Moderate-Resolution Imaging Spectroradiometer data. *Journal of Geophysical Research* 110, C07001, doi:10.1029/2004JC002560.
- Balestra, B., P. Ziveri, S. Monechi, and S. Troelstra, 2004. Coccolithophorids from the southeast Greenland margin (northern north Atlantic): Production, ecology, and the surface sediment record. *Micropaleontology* 50 (suppl. 1): 23-34.
- Barlow, R.G. and R.S. Alberte, 1985. Photosynthetic characteristics of phycoerythrin-containing marine *Synechococcus* spp. *Marine Biology*, 86, 63-74.
- Barlow, R.G., R.F.C. Mantoura, M.A. Gough, and T.W. Fileman, 1993. Pigment signatures of the phytoplankton composition in the northeastern Atlantic during the 1990 spring bloom. *Deep-Sea Research II*, 40, 459-477.
- Barlow, R.G., R.F.C. Mantoura, and D. Cummings, 1999. Monsoonal influences in the distribution of phytoplankton pigments in the Arabian Sea. *Deep-Sea Research II*, 46, 677-699.
- Bates, S.S. and T. Platt, 1984. Fluorescence induction as a measure of photosynthetic

- capacity in marine phytoplankton: response of *Thalassiosira pseudonana* (Bacillariophyceae) and *Dunaliella tertiolecta* (Chlorophyceae). *Marine Ecology Progress Series*, 18, 67-77.
- Bathmann, U.V., R. Scharek, C. Klaas, C.D. Dubischar, and V. Smetacek, 1997. Spring development of phytoplankton biomass and composition in major water masses of the Atlantic sector of the Southern Ocean. *Deep-Sea Research II*, 44, 51-67.
- Behrenfeld, M.J., Falkowski, P.G., 1997. Photosynthetic rates derived from satellite-based chlorophyll concentrations. *Limnology and Oceanography*, 42: 1-20.
- Ben-Amotz, A. and A. Gilboa, 1980. Cryptopreservation of marine unicellular algae. I. A survey of algae with regard to size, culture age, photosynthetic activity and chlorophyll – to - cell ratio. *Mar. Ecol. Prog. Ser.*, 2, 157-161.
- Blanchot, J., J.-M. Andre, C. Navarette, J. Neveux, and M.-H. Radenac, 2001. Picophytoplankton in the equatorial Pacific: Vertical distributions in the warm pool and in the high nutrient low chlorophyll conditions. *Deep-Sea Research I*, 48, 297-314.
- Boyd, P., A. Pomroy, S. Bury, G. Savidge, and I. Joint, 1997. Micro-algal carbon and nitrogen uptake in post-coccolithophore bloom conditions in the northeast Atlantic, July, 1991. *Deep-Sea Research I* 44, 1497-1517.
- Brand, L.E., W.G. Sunda, and R.R.L. Guillard, 1983. Limitation of marine phytoplankton reproductive rates by zinc, manganese, and iron. *Limnology and Oceanography*, 28, 1182-1198, 1983.
- Brand, L.E., W.G. Sunda, and R.R.L. Guillard, 1986. Reduction of marine phytoplankton reproduction rates by copper and cadmium. *Journal of Experimental Marine Biology and Ecology*, 96, 225-250.
- Bricaud, A., Morel, A., and L. Prieur, 1983. Optical efficiency factors of some phytoplankton. *Limnol. Oceanogr.* 28: 816-832.
- Bricaud, A. and A. Morel, 1986. Light attenuation and scattering by phytoplanktonic cells: a theoretical modeling. *Appl. Opt.* 25: 571-580.
- Bricaud, A., A.-L. Bedhomme, and A. Morel, 1988. Optical properties of diverse phytoplanktonic species: experimental results and theoretical interpretation. *J. Plank. Res.* 10: 851-873.
- Brown, C.W. and J.A. Yoder, 1994. Coccolithophorid blooms in the global ocean. *Journal of Geophysical Research* 99, 7467-7482.
- Brown, S.L. and M.R. Landry, 2001. Mesoscale variability in biological community structure and biomass in the antarctic polar front region at 170°W during austral spring 1997. *Journal of Geophysical Research*, 106, 13917-13930.
- Campbell, L., H. Liu, H.A. Nolla, and D. Vaultot, 1997. Annual variability of phytoplankton and bacteria in the subtropical North Pacific Ocean at Station ALOHA during the 1991-1994 ENSO event. *Deep-Sea Research I*, 44, 167-192.
- Carpenter, E.J. and K. Romans, 1991. Major role of the cyanobacterium *Trichodesmium* in nutrient cycling in the North Atlantic Ocean. *Science*, 254, 1356-1358.
- Carreto, J.I., N.G. Montoya, H.R. Benaidés, R. Guerrero, and M.O. Carignan, 2003. Characterization of spring phytoplankton communities in the Rio del La Plata maritime front using pigment signatures and cell microscopy. *Marine Biology* 143: 1013-1027.
- Claustre, H. and J.-C. Marty, 1995. Specific phytoplankton biomasses and their relation to primary production in the tropical North Atlantic. *Deep-Sea Research I*, 42, 1475-1493.

- Conkright, M.E., S. Levitus and T.P. Boyer, 1994. World Ocean Atlas, Volume 1: Nutrients, NOAA Atlas NESDIS 1, 150 pp.
- Conkright, M.E., Garcia, H.E., O'Brien, T.D., Locarnini, R.A., Boyer, T.P., Stephens, C., Antonov, J.I., 2002. World Ocean Atlas 2001, Volume 4: Nutrients. S. Levitus, Ed., NOAA Atlas NESDIS 52, U.S. Government Printing Office, Wash., D.C., 392 pp.
- Crawford, D.W., M.S. Lipsen, D.A. Purdie, M.C. Lohan, P.J. Statham, F.A. Whitney, J.N. Putland, W.K. Johnson, N. Sutherland, T.D. Peterson, P.J. Harrison, and C.S. Wong, 2003. Influence of zinc and iron enrichments on phytoplankton growth in the northeastern subarctic Pacific. *Limnology and Oceanography* 48: 1583-1600.
- Csanady, G.T., 1986. Mass transfer to and from small particles in the sea, *Limnol. Oceanogr.*, 31, 237-248.
- DiTullio, G.R., M.E. Geesey, D.R. Jones, K.L. Daly, L. Campbell, and W.O. Smith, 2003. Phytoplankton assemblage structure and primary productivity along 170°W in the South Pacific Ocean. *Marine Ecology Progress Series* 255: 55-80.
- DiTullio, G.R., M.E. Geesey, J.M. Maucher, M.B. Alm, S.F. Riseman, and K.W. Druland, 2005. Influence of iron on algal community composition and physiological status in the Peru upwelling system. *Limnology and Oceanography* 50: 1887-1907.
- Doney, S.C., K. Lindsay, K. Caldeira, J.-M. Campin, H. Drange, J.-C. Dutay, M. Follows, Y. Gao, A. Gnanadeskin, N. Gruber, A. Ishida, F. Joos, G. Madec, E. Maier-Reimer, J.C. Marshall, R.J. Matear, P. Monfray, A. Mouchet, R. Najjar, J.C. Orr, G.-K. Plattner, J. Sarmiento, R. Schlitzer, R. Slater, I.J. Totterdell, M.-F. Weirig, Y. Yamanaka, and A. Yool, 2004. Evaluating global ocean carbon models: The importance of realistic physics. *Global Biogeochemical Cycles* 18: 10.1029/2003GB002150.
- Dubinsky, Z. and T. Berman, 1986. Light utilization efficiencies of phytoplankton in Lake Kinneret (Sea of Galilee), *Limnol. Oceanogr.*, 21, 226-230.
- DuRand, M.D., R.J. Olson, and S.W. Chisholm, 2001. Phytoplankton population dynamics at the Bermuda Atlantic Time-series station in the Sargasso Sea. *Deep-Sea Research II*, 48, 1983-2003.
- Dutay, J.-C., J.L. Bullister, S.C. Doney, J.C. Orr, R. Najjar, K. Caldeira, J.-M. Campin, H. Drange, M. Follows, Y. Gao, N. Gruber, M.W. Hecht, A. Ishida, F. Joos, K. Lindsay, G. Madec, E. Maier-Reimer, J.C. Marshall, R.J. Matear, P. Monfray, A. Mouchet, G.-K. Plattner, J. Sarmiento, R. Schlitzer, R. Slater, I.J. Totterdell, M.-F. Weirig, Y. Yamanaka, and A. Yool, 2002. Evaluation of ocean model ventilation with CFC-11: Comparison of 13 global ocean models. *Ocean Modelling* 4: 89-120.
- Dutkiewicz, S., M.J. Follows, and P. Parekh, 2005. Interactions of the iron and phosphorus cycles: A three-dimensional model study. *Global Biogeochemical Cycles* 19: doi: 10.1029/2004GB002342.
- Enting, I.G., T. M. L. Wigley, M. Heimann, 1994. Future emissions and concentrations of carbon dioxide: key ocean/atmosphere/land analyses, CSIRO Aust. Div. Atmos. Res., Technical Paper No. 31, 118 pp.
- Eppley, R.W., J.N. Rogers, and J.J. McCarthy, 1969. Half-saturation constants for uptake of nitrate and ammonium by marine phytoplankton. *Limnology and Oceanography*, 14, 912-920.
- Eppley, R.W., 1972. Temperature and phytoplankton growth in the sea. *Fisheries Bulletin* 70, 1063-1085.

- Everitt, D., S. Wright, J.K. Volkman, D.P. Thomas, and E.J. Lindstrom, 1990. Phytoplankton community compositions in the western equatorial Pacific determined from chlorophyll and carotenoid pigment distributions. *Deep-Sea Research*, 37, 975-997.
- Falkowski, G., Z. Dubinsky, and K. Wyman, 1985. Growth-irradiance relationships in phytoplankton. *Limnology and Oceanography* 30, 311-321.
- Fritz, J.J. and W.M. Balch, 1996. A light-limited continuous culture study of *Emiliana huxleyi*: Determination of coccolith detachment and its relevance to cell sinking. *Journal of Experimental Marine Biology and Ecology* 207, 127-147.
- Fung, I.Y., S.K. Meyn, I. Tegen, S.C. Doney, J.G. John, and J.K.B. Bishop, 2000. Iron supply and demand in the upper ocean. *Global Biogeochemical Cycles*, 14, 281-295.
- Furnas, M.J., 1991. Net in situ growth rates of phytoplankton in an oligotrophic, tropical shelf ecosystem, *Limnol. Oceanogr.*, 36, 13-29.
- Gall, M.P., P.W. Boyd, J. Hall, K.A. Safi, and H. Chang, 2001. Phytoplankton processes. Part 1: Community structure during the Southern Ocean Iron Release Experiment (SOIREE). *Deep-Sea Research II*, 48, 2551-2570.
- Garrison, D.L., K. Buck, and M.M. Gowing, 1993. Winter plankton assemblage in the ice edge zone of the Weddell and Scotia Seas: Composition, biomass and spatial distribution. *Deep-Sea Research I*, 40, 311-338.
- Gavis, J., R.R.L. Guillard, and B.L. Woodward, 1981. Cupric ion activity and the growth of phytoplankton clones isolated from different marine environments. *Journal of Marine Research*, 39, 315-333.
- Gibb, S.W., D.G. Cummings, X. Irigoien, R.G. Barlow, R. Fauzi, and C. Mantoura, 2001. Phytoplankton pigment chemotaxonomy of the northeastern Atlantic. *Deep-Sea Research II*, 48, 795-823.
- Ginoux, P., M. Chin, I. Tegen, J.M. Prospero, B. Holben, O. Dubovik, and S.-J. Lin, 2001. Sources and distributions of dust aerosols simulated with the GOCART model. *Journal of Geophysical Research* 106, 20255-20273.
- Goericke, R., 2002. Top-down control of phytoplankton biomass and community structure in the monsoonal Arabian Sea. *Limnol. Oceanogr.* 47: 1307-1323.
- Goldman, J.C. and P.M. Glibert, 1982. Comparative rapid ammonium uptake by four species of marine phytoplankton, *Limnol. Oceanogr.*, 27, 814-827.
- Gregg, W.W. and K.L. Carder, 1990. A simple spectral solar irradiance model for cloudless maritime atmospheres. *Limnol. Oceanogr.* 35: 1657-1675.
- Gregg, W.W. and J.J. Walsh, 1992. Simulation of the 1979 spring bloom in the Mid-Atlantic Bight: A coupled physical/biological/optical model. *Journal of Geophysical Research* 97, 5723-5743.
- Gregg, W.W., 2002. A coupled ocean-atmosphere radiative model for global ocean biogeochemical models. NASA Global Modeling and Assimilation Series, M. Suarez, ed. NASA Technical Memorandum 2002-104606, Vol. 22, 33 pp. Available at [ftp://nsipp.gsfc.nasa.gov/CABIN/gregg/reprints/gregg\\_NASATM2002.pdf](ftp://nsipp.gsfc.nasa.gov/CABIN/gregg/reprints/gregg_NASATM2002.pdf).
- Gregg, W.W., P. Ginoux, P.S. Schopf, and N.W. Casey, 2003. Phytoplankton and Iron: Validation of a global three-dimensional ocean biogeochemical model. *Deep-Sea Research II* 50: 3143-3169.
- Hagino, K., H. Okada, and H. Matsuoka, 2000. Spatial dynamics of coccolithophore assemblages in the Equatorial Western-Central Pacific Ocean. *Marine*

- Micropaleontology 39: 53-72.
- Hardy, J., A. Hanneman, M. Behrenfeld, and R. Horner, 1996. Environmental biogeography of near-surface phytoplankton in the southeast Pacific Ocean. *Deep-Sea Research I*, 43, 1647-1659.
- Harris, R.P., P. Boyd, D.S. Harbour, R.N. Head, R.D. Pingree, and A.J. Pomroy, 1997. Physical, chemical and biological features of a cyclonic eddy in the region of 61°10'N 10°50'W in the North Atlantic. *Deep-Sea Research I*, 44, 1815-1839.
- Higgins, H.W. and D.J. Mackey, 2000. Algal class abundances, estimated from chlorophyll and carotenoid pigments, in the western Equatorial Pacific under El Niño and non-El Niño conditions. *Deep-Sea Research I*, 47, 1461-1483.
- Holligan, P.M., E. Fernandez, J. Aiken, W.M. Balch, P. Boyd, P.H. Burkill, M. Finch, S.B. Groom, G. Malin, K. Muller, D.A. Purdie, C. Robinson, C.C. Trees, S.M. Turner, and P. van der Waal, 1993. A biogeochemical study of the coccolithophore, *Emiliana huxleyi*, in the North Atlantic. *Global Biogeochemical Cycles*, 7, 879-900.
- Humphrey, G.F., 1979. Photosynthetic characteristics of algae grown under constant illumination and light-dark regimes, *J. Exp. Mar. Biol. Ecol.*, 40, 63-70.
- Hutchins, D.A., C.E. Hare, R.S. Weaver, Y. Zhang, G.F. Firme, G.R. Ditullio, M.B. Alm, S.F. Riseman, J.M. Maucher, M.E. Geesey, C.G. Trick, G.J. Smith, E.L. Rue, J. Conn, and K.W. Bruland, 2002. Phytoplankton iron limitation in the Humboldt Current and Peru upwelling. *Limnology and Oceanography* 47: 997-1011.
- Iglesias-Rodriguez, M.D., Brown, C.W., Doney, S.C., Kleypas, J., Kolber, D., Kolber, Z., Hayes, P.K., Falkowski, P.G., 2002. Representing key phytoplankton functional groups in ocean carbon cycle models: Coccolithophorids. *Global Biogeochemical Cycles*, 16 10.1029/2001BG001454.
- Ishizaka, J., K. Harada, K. Ishikawa, H. Kiyosawa, H. Furusawa, Y. Watanabe, H. Ishida, K. Suzuki, N. Handa, and M. Takahashi, 1997. Size and taxonomic plankton community structure and carbon flow at the equator, 175°E during 1990-1994. *Deep-Sea Research II*, 44, 1927-1949.
- Jin, X., N. Gruber, J.P. Dunne, J.L. Sarmiento, and R.A. Armstrong, 2006. Diagnosing CaCO<sub>3</sub> and opal export and phytoplankton functional groups from global nutrients and alkalinity distributions. *Global Biogeochemical Cycles*, in press.
- Kamykowski, D., S.-J. Zentara, J.M. Morrison, and A.C. Switzer, 2002. Dynamic global patterns of nitrate, phosphate, silicate, and iron availability and phytoplankton community composition from remote sensing data. *Global Biogeochemical Cycles* 16: doi: 10.1029/2001GB001640.
- Key, R.M., A. Kozyr, C.L. Sabin, K. Lee, R. Wanninkhof, J.L. Bullister, R.A. Feely, F.J. Millero, C. Mordy, and T.-H. Peng, 2004. A global ocean carbon climatology: Results from Global Data Analysis Project (GLODAP). *Global Biogeochemical Cycles* 18: 10.1029/2004GB002247.
- Kirk, J.T.O., 1980. Spectral properties of natural waters: Contribution of the soluble and particulate fractions to light absorption in some inland waters of southeastern Australia, *Australian Journal of Marine and Freshwater Research*, 31, 287-296.
- Lam, P.J., P.D. Tortell, and F.M.M. Morel, 2001. Differential effects of iron additions on organic and inorganic carbon production by phytoplankton. *Limnology and Oceanography* 46: 1199-1202.
- Landry, M.R., S.L. Brown, K.E. Selph, M.R. Abbott, R.M. Letelier, S. Christensen, R.R.

- Bidigare, and K. Casciotti, 2001. Initiation of the spring phytoplankton increase in the Antarctic polar front zone at 170° W. *Journal of Geophysical Research*, 106, 13903-13915.
- Landry, M.R., K.E. Selph, S.L. Brown, M.R. Abbott, C.I. Measures, S. Vink, C.B. Allen, A. Calbet, S. Christensen, and H. Nolla, 2002. Seasonal dynamics of phytoplankton in the Antarctic polar front region at 170° W. *Deep-Sea Research II* 49: 1843-1865.
- Langdon, C., 1987. On the causes of interspecific differences in the growth-irradiance relationship for phytoplankton. Part I. A comparative study of the growth-irradiance relationship of three marine phytoplankton species: *Skeletonema costatum*, *Olisthodiscus luteus*, and *Gonyaulax tamarensis*. *Journal of Plankton Research*, 9, 459-482.
- Le Quéré, C., and 19 others, 2005. Ecosystem dynamics based on plankton functional types for global ocean biogeochemistry models. *Global Change Biology* 11: 2016-2040.
- Letelier, R.M., R.R. Bidigare, D.V. Hebel, M. Ondrusek, C.D. Winn, and D.M. Karl, 1993. Temporal variability of phytoplankton community structure based on pigment analysis. *Limnology and Oceanography*, 38, 1420-1437.
- Malin, G., S. Turner, P. Liss, P. Holligan, and D. Harbour, 1993. Dimethylsulphide and dimethylsulphonioacetate in the Northeast Atlantic during the summer coccolithophore bloom. *Deep-Sea Research I*, 40, 1487-1508.
- Marañón, E., P.M. Holligan, M. Varela, B. Mourino, and A.J. Bale, 2000. Basin-scale variability of phytoplankton biomass and growth in the Atlantic Ocean. *Deep-Sea Research I*, 47: 825-857.
- Martin, J.H. and S.E. Fitzwater, 1988. Iron deficiency limits phytoplankton growth in the north-east Pacific. *Nature* 331 341-343.
- McGillicuddy, D.J., J.J. McCarthy, and A.R. Robinson, 1995. Coupled physical and biological modeling of the spring bloom in the North Atlantic (I): Model formulation and one dimensional bloom processes, *Deep-Sea Res.*, 42, 1313-1357, 1995.
- Miller, C.B., B.W. Frost, B. Booth, P.A. Wheeler, M.R. Landry, and N. Welschmeyer, 1991. Ecological processes in the subarctic Pacific: Iron limitation cannot be the whole story. *Oceanography* 4: 71-78.
- Mitchell, B.G. and D.A. Kiefer, 1988. Chlorophyll a specific absorption and fluorescence excitation spectra for light-limited phytoplankton, *Deep-Sea Res.*, 35, 639-663.
- Moore, J.K., S.C. Doney, J.A. Kleypas, D.M. Glover, and I.Y. Fung, 2002a. An intermediate complexity marine ecosystem model for the global domain. *Deep-Sea Research II* 49, 403-462.
- Moore, J.K., S.C. Doney, D.M. Glover, and I.Y. Fung, 2002b. Iron cycling and nutrient-limitation patterns in the surface waters of the world ocean. *Deep-Sea Research II* 49, 463-507.
- Moore, J.K., S.C. Doney, and K. Lindsay, 2004. Upper ocean dynamics and iron cycling in a global three-dimensional model. *Global Biogeochemical Cycles* 18: doi:10.2020/2004GB002220.
- Morel, A. 1987. Chlorophyll-specific scattering coefficient of phytoplankton. A simplified theoretical approach. *Deep-Sea Res.* 34: 1093-1105.
- Morel, A. and A. Bricaud, 1981. Theoretical results concerning light absorption in a discrete medium, and application to specific absorption of phytoplankton. *Deep-Sea*

- Res. 28: 1375-1393.
- Obayashi, Y., E. Tanoue, K. Suzuki, N. Handa, Y. Nojiri, and C.S. Wong, 2001. Spatial and temporal variabilities of phytoplankton community structure in the northern north Pacific as determined by phytoplankton pigments. *Deep-Sea Research I*, 48, 439-469.
- Peeken, I., 1997. Photosynthetic pigment fingerprints as indicators of phytoplankton biomass and development in different water masses of the Southern Ocean during austral spring. *Deep-Sea Research II*, 44, 261-282.
- Perry, M.J., M.C. Talbot, and R.S. Alberte, 1981. Photoadaptation in marine phytoplankton: response of the photosynthetic unit. *Marine Biology*, 62, 91-101.
- Robertson, J.E., C. Robinson, D.R. Turner, P. Holligan, A.J. Watson, P. Boyd, E. Fernandez, and M. Finch, 1994. The impact of a coccolithophore bloom on oceanic carbon uptake in the northeast Atlantic during summer 1991. *Deep-Sea Research I* 41, 297-314.
- Sakshaug, E. and K. Andresen, 1986. Effect of light regime upon growth rate and chemical composition of a clone of *Skeletonema costatum* from the Trondheimsfjord, Norway. *Journal of Plankton Research*, 8, 619-637.
- Sathyendranath, S., L. Lazzara, and L. Prieur, 1987. Variations in the spectral values of specific absorption of phytoplankton. *Limnol. Oceanogr.* 32: 403-415.
- Schopf, P.S. and A. Loughe, 1995. A reduced gravity isopycnal ocean model: Hindcasts of El Nino, *Mon. Wea. Rev.*, 123, 2839-2863.
- Steinberg, D.K., C.A. Carlson, N.R. Bates, R.J. Johnson, A.F. Michaels, and A.H. Knap, 2001. Overview of the US JGOFS Bermuda Atlantic Time-series Study (BATS): A decade-scale look at ocean biology and biogeochemistry. *Deep-Sea Research II*, 48, 1405-1447.
- Subba Rao, D.V., 1981. Growth response of marine phytoplankton to selected concentrations of trace metals, *Botanica marina*, 24, 369-379.
- Sunda, W.G. and S.A. Huntsman, 1995. Iron uptake and growth limitation in oceanic and coastal Phytoplankton. *Marine Chemistry*, 50, 189-206.
- Tarran, G.A., P.H. Burkill, E.S. Edwards, E. Malcolm, and S. Woodward, 1999. Phytoplankton community structure in the Arabian Sea during and after the SW monsoon, 1994. *Deep-Sea Research II*, 46, 655-676.
- Thibault, D., S. Roy, C.S. Wong, and J.K. Bishop, 1999. The downward flux of biogenic material in the NE subarctic Pacific: Importance of algal sinking and mesozooplankton herbivory. *Deep-Sea Research II*, 46, 2669-2697.
- van Leeuwe, M.A., H.J.W. DeBaar, and M.J.W. Veldhuis, 1998. Pigment distribution in the Pacific region of the southern ocean (autumn 1995). *Polar Biology*, 19, 348-353.
- Veldhuis, M.J.W. and G.W. Kraay, 2004. Phytoplankton in the tropical Atlantic Ocean: towards a better assessment of biomass and composition. *Deep-Sea Res. I* 51:507-530.
- Winter, A., M. Elbrachter, and G. Krause, 1999. Subtropical coccolithophores in the Weddell Sea. *Deep-Sea Research I* 46: 439-449.
- Wright, S.W., D.P. Thomas, H.J. Marchant, H.W. Higgins, M.D. Mackey, and D.J. Wu, J. and G.W. Luther, 1996. Spatial and temporal distribution of iron in the surface water of the northwestern Atlantic Ocean. *Geochimica et Cosmochimica Acta*, 60, 2729-2741.
- Wright, S.W. and R.L. van den Enden, 2000. Phytoplankton community structure and stocks in the East Antarctic marginal ice zone (BROKE survey, January-March 1996)

determined by CHEMTAX analysis of HPLC pigment signatures. *Deep-Sea Research II* 47: 2363-2400.

Wyman, M. and P. Fay, 1986. Underwater light climate and the growth and pigmentation of planktonic blue-green algae (Cyanobacteria) I. The influence of light quantity.

*Proceedings of the Royal Society of London*, 227, 367-380.

Yang, T.-N., K.-Y. Wei, and G.-C. Gong, 2001. Distribution of coccolithophorids and coccoliths in surface ocean off northeastern Taiwan. *Botanical Bulletin of the Academia Sinica* 42: 287-302.



## Appendix. Biogeochemical processes model description.

NOBM is based on Gregg et al. (2003). There are several new features in the biogeochemical processes model component:

- full, integrated dissolved organic and inorganic carbon components and cycling
- new maximum phytoplankton growth rates at 20°C, to represent gross growth rates rather than net
- full detrital dynamics with 3 components, fully coupled to the OGCM
- a new formulation for the temperature-dependence for grazing
- a new formulation for nitrogen fixation for the cyanobacteria component
- introduction of dissolved iron scavenging and an increase in atmospheric iron solubility
- new nitrogen half-saturation constants for chlorophytes
- new iron half-saturation constants for chlorophytes and cyanobacteria
- reduced sinking rate for diatoms

Other aspects of the biogeochemical processes model are described in Gregg et al (2003), but are provided here for completeness.

The governing equations of the model are

### *Phytoplankton*

$$\frac{\partial}{\partial t} P_i = \nabla(K\nabla P_i) - \nabla \bullet \mathbf{V} P_i - \nabla \bullet (\mathbf{w}_s)_i P_i + [\mu_i - (\delta + \Omega)] P_i - \gamma H - \kappa P_i \quad (\text{A1})$$

- i = 1 = diatoms
- i = 2 = chlorophytes
- i = 3 = cyanobacteria
- i = 4 = coccolithophores

### *Nutrients*

$$\frac{\partial}{\partial t} N_N = \nabla(K\nabla N_N) - \nabla \bullet \mathbf{V} N_N - b_N [\sum_i \mu_i P_i] + R\alpha_C D_C / (C:N) + \lambda_D D_C / (C:N) \quad (\text{A2})$$

$$\frac{\partial}{\partial t} N_A = \nabla(K\nabla N_A) - \nabla \bullet \mathbf{V} N_A - b_N [\sum_i \mu_i P_i] + b_N \epsilon [\gamma H + n_2 H^2] \quad (\text{A3})$$

$$\frac{\partial}{\partial t} N_S = \nabla(K\nabla N_S) - \nabla \bullet \mathbf{V} N_S - b_S \mu_1 P_1 + R\alpha_S D_S \quad (\text{A4})$$

$$\frac{\partial}{\partial t} N_F = \nabla(K\nabla N_F) - \nabla \bullet \mathbf{V} N_F - b_F [\sum_i \mu_i P_i] + b_F \epsilon [\gamma H + \eta_2 H^2] + R\alpha_F D_F + A_{Fe}/L - \theta N_F \quad (\text{A5})$$

$N_N$  = nitrate  
 $N_A$  = ammonium  
 $N_S$  = silica  
 $N_F$  = dissolved iron

*Herbivores*

$$\frac{\partial}{\partial t} H = \nabla(K\nabla H) - \nabla \bullet \mathbf{V}H + (1-\varepsilon)\gamma H - \eta_1 H - \eta_2 H^2 - \omega H - \Theta H \quad (A6)$$

*Detritus*

$$\frac{\partial}{\partial t} D_C = \nabla(K\nabla D_C) - \nabla \bullet \mathbf{V}D_C - \nabla \bullet (\mathbf{w}_d)_C D_C - R\alpha_N D_C + \Phi[\kappa \Sigma_i P_i + \eta_1 H] + \Phi(1-\varepsilon) \eta_2 H^2 - \lambda_D D_C \quad (A7)$$

$$\frac{\partial}{\partial t} D_S = \nabla(K\nabla D_S) - \nabla \bullet \mathbf{V}D_S - \nabla \bullet (\mathbf{w}_d)_S D_S - R\alpha_S D_S + b_S[\kappa P_1 + \gamma H] \quad (A8)$$

$$\frac{\partial}{\partial t} D_F = \nabla(K\nabla D_F) - \nabla \bullet \mathbf{V}D_F - \nabla \bullet (\mathbf{w}_d)_F D_F - R\alpha_F D_F + b_F[\kappa \Sigma_i P_i + \eta_1 H] + b_F(1-\varepsilon) \eta_2 H^2 + \theta N_F \quad (A9)$$

$D_C$  = carbon/nitrogen detritus  
 $D_S$  = silica detritus  
 $D_F$  = iron detritus

*Carbon*

$$\frac{\partial}{\partial t} \text{DOC} = \nabla(K\nabla \text{DOC}) - \nabla \bullet \mathbf{V}\text{DOC} + \Phi \delta \Sigma \mu_i P_i + \Phi \omega H + \lambda_D D_C - \phi \text{DOC} \quad (A10)$$

$$\frac{\partial}{\partial t} \text{DIC} = \nabla(K\nabla \text{DIC}) - \nabla \bullet \mathbf{V}\text{DIC} - \Phi \Sigma \mu_i P_i + \Phi \Omega \Sigma \mu_i P_i + \Phi \Theta H + \phi \text{DOC} + R\alpha_N D_C / (C:N) + A_{O_{CO2}} \quad (A11)$$

where the symbols and values are identified in Appendix Table 1. Bold denotes a vector quantity. All biological processes are assumed to cease in the presence of sea ice, in proportion to the fraction of sea ice cover, which is included as an external forcing field.

### ***Circulation Model***

The Ocean General Circulation Model (OGCM) is a reduced gravity representation of circulation fields (Schopf and Lough, 1995). It is global in scale, extending from near the South Pole to 72° N, in increments of 2/3° latitude and 1 1/4° longitude, comprising all regions where bottom depth > 200m. The model contains 14 vertical layers, in quasi-isopycnal coordinates, and is driven by wind stress, sea surface temperature, and shortwave radiation.

### ***Radiative Model***

Radiative transfer calculations provide the underwater irradiance fields necessary to drive growth of the phytoplankton groups, and interact with the heat budget. The Ocean-Atmosphere Radiative Model (OARM; Gregg, 2002) contains a treatment of the spectral and directional properties of radiative transfer in the oceans, and explicitly accounts for clouds. The atmospheric radiative model is based on the Gregg and Carder (1990) spectral model, extended to the spectral regions 200 nm to 4 µm. It requires external monthly climatologies of cloud properties (cloud cover and liquid water path), surface pressure, wind speeds, relative humidity, precipitable water, and ozone. Aerosols are considered to be strictly of marine origin and are computed as in Gregg and Carder (1990).

Oceanic radiative properties are driven by water absorption and scattering, the optical properties of the phytoplankton groups, and chromophoric dissolved organic matter (CDOM). Three irradiance paths are enabled: a downwelling direct path, a downwelling diffuse (scattered) path, and an upwelling diffuse path. All oceanic radiative calculations include the spectral nature of the irradiance.

Optical properties of coccolithophores and other phytoplankton groups were derived from laboratory studies. Their values and references can be found in Gregg (2002).

### ***Phytoplankton***

The growth formulation includes dependence on total irradiance ( $E_T$ ), nitrogen as nitrate plus ammonium ( $N_T$ ), silica ( $Si$  – for diatoms only), iron ( $Fe$ ), and temperature ( $T$ )

$$\mu_i = \mu_{mi} \min[\mu(E_T)_i, \mu(N_T)_i, \mu(Si)_i, \mu(Fe)_i] RG_i \quad (A12)$$

where  $i$  indicates the phytoplankton functional group index (in order, diatoms, chlorophytes, cyanobacteria, and coccolithophores),  $\mu$  is the total specific growth rate ( $d^{-1}$ ) of phytoplankton,  $\mu_m$  is the maximum growth rate at 20°C (Appendix Table 1). The term  $\mu(E_T)$  represents the growth rate as a function solely of the total irradiance ( $\mu mol \text{ quanta } m^{-2} s^{-1}$ ),

$$\mu(E_T) = \frac{E_T}{(E_T + k_E)} \quad (A13)$$

where  $k_E$  is the irradiance at which  $\mu = 0.5\mu_m$  and equals  $0.5 I_k$ , where  $I_k$  is the light saturation parameter. The nutrient-dependent growth terms are

$$\mu(NO_3)_i = \frac{NO_3}{[NO_3 + (k_N)_i]} \quad (A14)$$
$$NH_4$$

$$\mu(\text{NH}_4)_i = \frac{\text{Si}}{[\text{NH}_4 + (k_N)_i]} \quad (\text{A15})$$

$$\mu(\text{N}_T)_i = \mu(\text{NH}_4)_i + \min[\mu(\text{NO}_3)_i, 1 - \mu(\text{NH}_4)_i] \quad (\text{A16})$$

(Gregg and Walsh, 1992)

$$\mu(\text{Si})_i = \frac{\text{Si}}{[\text{Si} + (k_S)_i]} \quad (\text{A17})$$

$$\mu(\text{Fe})_i = \frac{\text{Fe}}{[\text{Fe} + (k_F)_i]} \quad (\text{A18})$$

Temperature-dependent growth is from Eppley (1972)

$$R = 1.066^{(T-20)} \quad (\text{A19})$$

which produces a temperature-growth factor normalized to 20°C. The term G in Eq. A12 is an additional adjustment used for the cyanobacteria component that reduces their growth rate in cold water (<15°C)

$$G_3 = 0.0294T + 0.558 \quad (\text{A20})$$

$G_i = 1$  for the other three phytoplankton components ( $i=1,2,4$ ). When  $T \geq 15^\circ\text{C}$ ,  $G_3$  reaches its maximum value of 1. This effect conforms to observations that cyanobacteria are scarce in cold waters (Agawin et al., 2000; 1998).

The cyanobacteria component possesses a modest ability to fix nitrogen from the water column, as observed in *Trichodesmium* spp. (Carpenter & Romans 1991). The nitrogen fixation is expressed as additional growth occurring when nitrogen availability is  $< (k_N)_3$ ,

$$\mu_{\text{fix}} = 0.25 \exp(-75P_3) \quad (\text{A21})$$

where the index 3 indicates cyanobacteria. The biomass dependence represents a progressive community changeover from non-N-fixing cyanobacteria to N-fixing bacteria as the total population declines under nitrogen-stressed conditions. The total N-limited growth rate plus the additional growth derived from N-fixation is not allowed to exceed the growth rate where total nitrogen =  $(k_N)_3$ . No accounting for denitrification is made in the model.

Photoadaptation is simulated by stipulating 3 states: 50, 150 and 200 ( $\mu\text{mol quanta m}^{-2} \text{ s}^{-1}$ ). This is based on laboratory studies which typically divided experiments into low, medium, and high classes of light adaptation. Carbon:chlorophyll ratios ( $\Phi$ ) correspond to the photoadaptation state, to represent the tendency of phytoplankton to preferentially synthesize chlorophyll in low light conditions, to enable more efficient photon capture. The three  $\Phi$  states corresponding to the three light states are 25, 50 and 80  $\text{g g}^{-1}$ . The  $\Phi$  results for diatoms in the model closely mimic Anning et al.'s (2000) results for diatoms. For irradiance levels falling between the three light states, the C:chl ratios are linearly interpolated.

Mean irradiance is computed during daylight hours, and then the phytoplankton photoadaptive state is classified accordingly. This calculation is only performed once per day to simulate a

delayed photoadaptation response. Light saturation constants for the three light levels are provided in Appendix Table 1.

Phytoplankton group physiological parameters  $\mu_m$ ,  $I_k$ , and  $k_{N,S,F}$  are derived from carefully controlled, inter-comparative laboratory studies. We require that at least two of the groups are involved simultaneously in order to utilize the experimental results. For  $\mu_m$  mean values of the relative growth rates are derived from the results of Ben-Amotz and Gilboa (1980), Brand et al. (1986, 1983), Eppley et al. (1969), Falkowski et al. (1985), Furnas (1991), Gavis et al. (1981), Goldman and Glibert (1982), Humphrey (1979), Subba Rao (1981), and Sunda and Huntsman (1995).

Light saturation parameters,  $I_k$ , are formulated for the three irradiance categories used to define photoadaptation. Mean values are summarized from the reports of Barlow and Alberte (1985), Bates and Platt (1984), Langdon (1987), Perry et al. (1981), Sakshaug and Andresen (1986), and Wyman and Fay (1986).

The coccolithophore half-saturation constant for nitrogen ( $k_N$ ) was observed by Eppley (1969) to be one-half the value of diatoms. Cyanobacteria  $k_N$  is set slightly lower than coccolithophores, assuming small particle size leads to improved nutrient uptake efficiency. Chlorophyte  $k_N$  is set at one-third the departure between diatoms and coccolithophores. The diatom  $k_N$  is arbitrarily set to 1  $\mu\text{M}$ .

Phytoplankton vector sinking is treated as additional advection in the z-direction. Sinking rates are specified at 31°C and derived from Stokes Law using representative phytoplankton sizes from Ahn et al. (1992), Bricaud and Morel (1986), Bricaud et al. (1983; 1988), Dubinsky and Berman (1986), Kirk (1980); Mitchell and Kiefer (1988), Morel (1987), Morel and Bricaud (1981), and Sathyendranath et al. (1987), for the individual groups. The rates are adjusted by viscosity according to Stokes Law (Csanady, 1986), which is parameterized here by temperature

$$w_s(T) = w_s(31)[0.451 + 0.0178T] \quad (\text{A22})$$

Coccolithophore sinking rates are allowed to vary as a function of growth rate from 0.3 to 1.4  $\text{m d}^{-1}$  based on observations by Fritz and Balch (1996). A linear relationship is assumed

$$w_{s4} = 0.752\mu_4(\text{high}) + 0.225 \quad (\text{A23})$$

where  $w_s$  is the sinking rate of coccolithophores ( $\text{m d}^{-1}$ ),  $\mu(\text{high})$  is the highest growth rate actually achieved for the previous day, and the subscript 4 represents coccolithophores.

### **Nutrients**

The diversity in the processes affecting the four nutrient groups requires elucidation in 4 separate equations, unlike the phytoplankton. All are taken up by phytoplankton growth, with silica subject only to diatom uptake (note the subscript=1 in Eq. A4 denoting diatoms). For three of the nutrients, nitrate, silica, and dissolved iron, corresponding detrital pools remineralize to return nutrients previously uptaken by phytoplankton. There is no detrital pool for ammonium, which is excreted as a function of herbivore grazing, and as a function of higher order ingestion of herbivores, represented by the term  $n_2H^2$  in Eqs. A3, A5, A6, A7, and A9. Dissolved iron also has an excretion pathway, but nitrate and silica do not. The nutrient to chlorophyll ratios, denoted  $b$  in Eqs. A2-A5, are derived from Redfield ratios, which are constant (Appendix Table 1) and the carbon:chlorophyll ( $\Phi$ ) ratio which is not.

$$b_N = \Phi/C:N \quad (\text{A24})$$

$$b_S = \Phi/C:S \quad (A25)$$

$$b_F = \Phi/C:Fe \quad (A26)$$

This leads to variable nutrient to chlorophyll ratios in the model.

As in Gregg et al. (2003) dust deposition fields are derived from Ginoux et al. (2001). In this model, four dust size fractions are transported, corresponding to clay (smallest) and three increasing fractions of silt. The iron content is assumed to vary among the clay and silt fractions as follows: clay = 3.5% iron, silt = 1.2% iron (Fung et al., 2000). Iron solubility is assumed at 2% for all fractions, which is toward the low end of current estimates (Fung et al., 2000), but is the same as used by Moore et al. (2004). The bottom boundary condition is 0.6 nM (Archer and Johnson, 2000)

Iron scavenging is implemented in this version of NOBM. It is set at  $2.74 \times 10^{-5} \text{ d}^{-1}$  at low iron concentrations ( $< 0.6 \text{ nM}$ ; Moore et al., 2002b) and 50 times this rate at higher concentrations. A smooth transition is enabled as in Moore et al. (2002b)

$$\theta = 2.74 \times 10^{-5} N_F, \text{ for } N_F < 0.6 \text{ nM} \quad (A27)$$

$$\theta = 2.74 \times 10^{-5} N_F + 1.37 \times 10^{-3} (N_F - 0.6), \text{ for } N_F \geq 0.6 \text{ nM} \quad (A28)$$

### ***Herbivores***

Grazing uses an Ivlev formulation (McGillicuddy et al., 1995),

$$\gamma(T) = \gamma_m R_H [1 - \exp(-\Lambda \sum_i P_i)] \quad (A29)$$

$R_H$  is the maximum grazing rate at  $20^\circ \text{ C}$  ( $\gamma_m$ ) adjusted by temperature

$$R_H = 0.06 \exp(0.1T) + 0.70 \quad (A30)$$

The temperature-dependence for grazing is more linear than that for phytoplankton, reflecting the larger size of their overall community. The grazing represents the total loss of phytoplankton to herbivores, as indicated by the summation symbol, but is applied to the individual phytoplankton functional groups proportionately to their relative abundances. This enables herbivore grazing to self-adapt the prevailing phytoplankton community.

The two loss terms in Eq. A6 represent the death of herbivores ( $\eta_1 H$ ) and higher order heterotrophic losses ( $\eta_2 H^2$ ). These formulations and parameters (Appendix Table 1) were taken from McGillicuddy et al. (1995).

### ***Detritus***

Three detrital components represent the three major nutrient elements, carbon/nitrogen, silica, and iron (Eq. A6-A9). The nitrogen detritus is kept as carbon in the model, but since the C:N ratio is constant, it is simple to convert when needed. All are subject to advection, diffusion and sinking. Detrital sinking, like phytoplankton sinking, is dependent on viscosity parameterized here in terms of temperature, using the same formulation. Remineralization,  $\kappa$ , is also temperature-dependent, and uses the phytoplankton growth-dependence term  $R$  in Eq. A19. Silica contained in the diatom component of phytoplankton is assumed to pass through herbivores upon grazing directly into the silica detritus pool. No silica remains in the herbivore component at any time.

### ***Carbon***

Dissolved organic carbon cycling is taken from Aumont et al. (2002), with conversions added for compatibility with NOBM units. In addition, all parameters are temperature-dependent, unlike Aumont et al. (2002), using the phytoplankton temperature dependence defined in Eq. A19. Following Aumont et al. (2002), excretion of DOC by the herbivore component is

$$\omega = r_H \frac{H}{H_0 + H} R \quad (A31)$$

where  $r_H$  is the herbivore excretion rate at 20°C, and  $H_0$  is the half-saturation constant for excretion (Appendix Table 1).  $H_0$  is adjusted from units of  $\mu\text{M}$  carbon in Aumont et al. (2002) to  $\text{mg m}^{-3}$  chlorophyll to conform to the NOBM units for herbivores. Bacterial degradation of DOC is represented by

$$\phi = \lambda_{\text{DOC}} \frac{N_1}{K_1 + N_1} \frac{\text{DOC}}{K_2 + \text{DOC}} \text{DOC} R \quad (A32)$$

where  $\lambda_{\text{DOC}}$  is the DOC remineralization rate and  $K_1$  and  $K_2$  are half-saturation constants for remineralization (Aumont et al., 2002; Appendix Table 1). Aumont et al. (2002) used phosphate, so here we substitute nitrate, since phosphate is not available in NOBM. Again parameters are allowed to vary as a function of temperature. In addition, the value for  $K_1$  was increased by a factor of 10 to convert to nitrate rather than phosphate. According to Conkright et al. (1994), nitrate contours generally follow phosphate but nitrate concentrations are approximately 10 times higher.

Dissolved inorganic carbon has a single sink, uptake by phytoplankton during photosynthesis, and sources deriving from respiration by phytoplankton  $\Omega$  in the process of growth, herbivores  $\Theta$  at all times, and bacteria  $\phi$  in the process of degrading DOC. There is also an interaction with the atmosphere ( $\text{AO}_{\text{CO}_2}$ ) which can be a source or a sink depending upon the difference in partial pressures of  $\text{CO}_2$  in the ocean and atmosphere ( $\Delta p_{\text{CO}_2}$ ), and the ability for gas to transfer across the ocean surface interface. These complex processes are follow procedures described by the Ocean Carbon Model Intercomparison Project (Dutay et al., 2002; Doney et al., 2004; <http://www.ipsl.jussieu.fr/OCMIP/>).

### ***Initial Conditions***

NOBM underwent a spin-up of a total of 35 years under climatological forcing. For the first 15 years, initial dissolved iron conditions were from Fung et al. (2000), and nitrate and silica distributions were from annual climatologies from National Oceanographic Data Center (NODC; Conkright et al., 2002). Ammonium initial conditions were set to  $0.5\mu\text{M}$ . Initial conditions for all phytoplankton groups and herbivores were set to  $0.05 \text{ mg m}^{-3}$  chl throughout the entire model domain. Initial conditions for detritus were set to 0. Initial conditions for DIC were taken from Key et al., (2004). Mean global values by depth were computed and used as initial conditions. After 15 years, dissolved iron, detritus, DIC and DOC distributions were retained, while all other fields were reset to their original values. The model was run again for 20 years. This methodology enables dissolved iron to reach steady state without adversely impacting phytoplankton group distributions with excessively low initial values.

Appendix Table 1. Notation, parameters, and variables for NOBM. Values are provided for the parameters and ranges are provided for the variables. When a parameter varies according to temperature, the value at a specified temperature is shown and identified. Nutrient/chlorophyll ratios are variable because of photadaptation-dependence, and only the range is shown, corresponding to low-, and high-light adaptation, and therefore also corresponding to C:chl ratios of 20 and 80 g g<sup>-1</sup>.

Symbol	Parameter/Variable	Value	Units
<i>General</i>			
K	Diffusivity	Variable	m <sup>2</sup> s <sup>-1</sup>
∇	Gradient operator	none	none
V	Vector velocity	Variable	m s <sup>-1</sup>
L	Layer thickness	Variable	m
<i>Phytoplankton</i>			
w <sub>s</sub>	Vector sinking rate of phytoplankton at 31°C		m d <sup>-1</sup>
	diatoms	0.75	
	chlorophytes	0.25	
	cyanobacteria	0.0085	
	coccolithophores	0.3-1.4	
μ	Specific growth rate of phytoplankton		d <sup>-1</sup>
	maximum (μ <sub>m</sub> ) at 20°C:		
	diatoms	1.50	
	chlorophytes	1.26	
	cyanobacteria	1.00	
	coccolithophores	1.13	
I <sub>k</sub>	Light Saturation		μmol quanta m <sup>-2</sup> s <sup>-1</sup>
	Light level: Low (50)	Medium (150)	High (200)
	diatoms 90.0	93.0	184.0
	chlorophytes 96.9	87.0	143.7
	cyanobacteria 65.1	66.0	47.0
	coccolithophores 56.1	71.2	165.4
κ	Senescence rate	0.05	d <sup>-1</sup>
k <sub>E</sub>	Half-saturation for growth as function of quanta	0.5I <sub>k</sub>	μmol quanta m <sup>-2</sup> s <sup>-1</sup>
E <sub>T</sub>	Total quanta (direct+diffuse)	variable	μmol quanta m <sup>-2</sup> s <sup>-1</sup>
R	Temperature dependence for growth	0.25-9.4	none
G	Temperature-dependence for cyanobacteria growth	0.5-1.0	none
<i>Nutrients (N)</i>			
b <sub>N,S,F</sub>	Nutrient:chlorophyll ratio		μM (μg l <sup>-1</sup> ) <sup>-1</sup>
	nitrogen	0.3 – 1.0	
	silica	0.3 – 1.0	
	iron	0.01 – 0.04	
ε	Nutrient excretion		d <sup>-1</sup>



	nitrate	0.0	
	ammonium	0.25	
	silica	0.0	
	iron	0.25	
$k_{N,S,F}$	Half-saturation constant		
	nitrogen/carbon		$\mu\text{M}$
	diatoms	1.0	
	chlorophytes	0.67	
	cyanobacteria	0.45	
	coccolithophores	0.50	
	silica		$\mu\text{M}$
	diatoms	0.2	
	iron		$\text{nM}$
	diatoms	1.0	
	chlorophytes	0.78	
	cyanobacteria	0.67	
	coccolithophores	0.67	
$\theta$	Iron scavenging rate		$\text{d}^{-1}$
	Low iron ( $<0.06\text{nM}$ )	$2.74 \times 10^{-5}$	
	High iron ( $\geq 0.06\text{nM}$ )	$1.37 \times 10^{-3}$	
$A_{\text{Fe}}$	Atmospheric deposition of iron	0.03-967.0	$\text{nmol m}^{-2} \text{d}^{-1}$
C:N	Carbon:nitrogen ratio	79.5	$\mu\text{g l}^{-1} (\mu\text{M})^{-1}$
C:S	Carbon:silica ratio	79.5	$\mu\text{g l}^{-1} (\mu\text{M})^{-1}$
C:Fe	Carbon:iron ratio	1800	$\mu\text{g l}^{-1} (\text{nM})^{-1}$
<i>Herbivores (H)</i>			
$\gamma$	Grazing rate		
	maximum ( $\gamma_m$ ) at $20^\circ\text{C}$	1.2	$\text{d}^{-1}$
$\Lambda$	Ivlev constant	1.0	$(\mu\text{g l}^{-1})^{-1}$
$\eta_1, \eta_2$	Heterotrophic loss rates	0.1, 0.5	$\text{d}^{-1}$
$R_H$	Temperature-dependence for grazing	0.75-2.7	none
<i>Detritus (D)</i>			
$w_d$	Vector sinking rate of detritus at $31^\circ\text{C}$		$\text{m d}^{-1}$
	carbon/nitrogen detritus	30.0	
	silica detritus	50.0	
	iron detritus	20.0	
$\alpha_{C,S,F}$	Remineralization rate at $20^\circ\text{C}$		$\text{d}^{-1}$
	carbon/nitrate	0.01	
	silica	0.0001	
	iron	0.02	
$\Phi$	Carbon:chlorophyll ratio	Variable	$\text{g g}^{-1}$

*Carbon (DOC, DIC)*

$\delta$	Phytoplankton DOC exudation fraction	0.05	none
$r_H$	Excretion rate of DOC by herbivores at 20°C	0.05	d <sup>-1</sup>
$H_o$	Half-saturation constant for herbivore excretion of DOC	0.14	mg m <sup>-3</sup>
$\lambda_D$	Detrital breakdown rate at 20°C	0.05	d <sup>-1</sup>
$\lambda_{DOC}$	Remineralization rate of DOC to nitrate	0.017	d <sup>-1</sup>
$\omega$	Herbivore excretion function for DOC	variable	d <sup>-1</sup>
$\Omega$	Phytoplankton respiration fraction	0.05	none
$\Theta$	Herbivore respiration	0.05	d <sup>-1</sup>
$\Phi$	Bacterial degradation of DOC to DIC	variable	d <sup>-1</sup>
$K_1$	First half-saturation constant for remineralization to nitrate	3.0	μM
$K_2$	Second half-saturation constant for remineralization to nitrate	15.0	μM
$AO_{CO_2}$	Atmospheric-oceanic CO <sub>2</sub> equilibration	Variable	μatm